

GRAPH-BASED JOINT CHANNEL ESTIMATION AND DATA DETECTION
FOR LARGE-SCALE MULTIUSER MIMO-OFDM SYSTEMS

A THESIS SUBMITTED TO
THE GRADUATE SCHOOL OF NATURAL AND APPLIED SCIENCES
OF
MIDDLE EAST TECHNICAL UNIVERSITY

BY

ŞEREF YAŞAR TEKİN

IN PARTIAL FULFILLMENT OF THE REQUIREMENTS
FOR
THE DEGREE OF MASTER OF SCIENCE
IN
ELECTRICAL AND ELECTRONICS ENGINEERING

MARCH 2015

Approval of the thesis:

**GRAPH-BASED JOINT CHANNEL ESTIMATION AND DATA DETECTION
FOR LARGE-SCALE MULTIUSER MIMO-OFDM SYSTEMS**

submitted by **ŞEREF YAŞAR TEKİN** in partial fulfillment of the requirements for the degree of **Master of Science in Electrical and Electronics Engineering Department, Middle East Technical University** by,

Prof. Dr. Gülbin Dural Ünver
Dean, Graduate School of **Natural and Applied Sciences**

Prof. Dr. Gönül Turhan Sayan
Head of Department, **Electrical and Electronics Engineering**

Prof. Dr. Ali Özgür Yılmaz
Supervisor, **Electrical and Electronics Eng. Dept., METU**

Examining Committee Members:

Prof. Dr. Yalçın Tanık
Electrical and Electronics Engineering Dept., METU

Prof. Dr. Ali Özgür Yılmaz
Electrical and Electronics Engineering Dept., METU

Prof. Dr. Buyurman Baykal
Electrical and Electronics Engineering Dept., METU

Prof. Dr. Tolga M. Duman
Electrical and Electronics Engineering Dept., Bilkent University

Assoc. Prof. Dr. Melek Diker Yücel
Electrical and Electronics Engineering Dept., METU

Date:

I hereby declare that all information in this document has been obtained and presented in accordance with academic rules and ethical conduct. I also declare that, as required by these rules and conduct, I have fully cited and referenced all material and results that are not original to this work.

Name, Last Name: ŞEREF YAŞAR TEKİN

Signature :

ABSTRACT

GRAPH-BASED JOINT CHANNEL ESTIMATION AND DATA DETECTION FOR LARGE-SCALE MULTIUSER MIMO-OFDM SYSTEMS

Şeref Yaşar Tekin,

M.S., Department of Electrical and Electronics Engineering

Supervisor : Prof. Dr. Ali Özgür Yılmaz

March 2015, 52 pages

In this thesis, a graph-based soft iterative receiver for large-scale multiuser MIMO-OFDM systems is proposed that performs joint channel estimation and data detection over time-varying frequency selective channel. In an uplink scenario, factor graph structures for the transmitter of users and the receiver of base-station are presented, which provide Gaussian message passing between nodes. Instead of LLR, reliability information of symbols are used to decrease complexity of the proposed algorithm. Training symbols, known at the receiver, are utilized to get channel state information at the initialization. Also a new training structure is proposed which enables channel estimation and data detection for numerous users. Soft channel estimation process is introduced which utilizes correlation information between channel coefficients. Transfer nodes bring reliability information of channel coefficients between coefficient nodes to converge actual value. Message passing schedule is rearranged to enhance performance of the graph based soft iterative receiver. Extrinsic information exchange is applied between nodes of the repeated symbols. Soft information of the channel coefficients and symbols are jointly refined in each iteration.

The BER performance analysis of graph based soft iterative receiver is investigated by comparing non-iterative ML and MRC. Simulation results show that the proposed algorithm with channel knowledge has a similar performance with MRC and outperforms non-iterative ML. Performance of GSIR with different training symbol spac-

ing, number of users, number of receive antennas, code rates and constellations are compared to provide an overview of the proposed algorithm. Also channel estimation performance of GSIR is analyzed by comparing with perfect channel knowledge case. A LDPC decoder is used in combination with GSIR to increase total performance.

Keywords: MIMO-OFDM, factor graph, Gaussian message passing, channel estimation, iterative receiver, fading channels, BER Analysis

ÖZ

ÇOK KULLANICILI BÜYÜK ÖLÇEKLİ MIMO-OFDM SİSTEMLER İÇİN ÇARPAN ÇİZGE TEMELLİ BİRLEŞİK KANAL KESTİRİMİ VE VERİ TESPİTİ

Şeref Yaşar Tekin,

Yüksek Lisans, Elektrik ve Elektronik Mühendisliği Bölümü

Tez Yöneticisi : Prof. Dr. Ali Özgür Yılmaz

Mart 2015 , 52 sayfa

Bu tezde, frekans seçici zamanla değişen kanallarda çok kullanıcıli büyük ölçekli MIMO-OFDM sistemler için çarpın çizge temelli yinelemeli bir alıcı yapısı öne sürülmüştür. Kullanıcıdan baz istasyonuna iletişim durumunda, kullanıcıların göndericisi ve baz istasyonu alıcısı için sunulan çizge yapısı Gauss mesaj iletimi ile çalışmaktadır. Sunulan algoritmanın karmaşıklığını azaltmak için LLR yerine sembollerin güvenilirlik bilgisi kullanılmıştır. Başlangıç durumunda kanal durum bilgisini elde etmek için alıcıda bilinen örnek semboller kullanılmıştır. Ayrıca, çok sayıda kullanıcı için kanal kestirimi ve veri tespitine olanak sağlayan yeni bir örnek sembolleme yapısı önerilmiştir. Kanal katsayıları arasındaki bağıntı bilgisini kullanan kanal kestirimi süreci tanımlanmıştır. Nakil boğumları kanal katsayılarının güvenilirlik bilgisini kanal boğumları arasında taşıyarak kanal katsayılarına ulaşılmasını sağlar. Çarpın çizge temelli yinelemeli alıcının performansını arttırmak için mesaj iletimi planı yeniden ayarlanmıştır. Harici bilgi değişimi tekrarlanmış sembol boğumları arasında uygulanır. Kanal katsayıları ve sembollerin bilgisi her yinelemede birlikte artırılır.

Yinelemesiz ML ve MRC algoritmaları ile karşılaştırarak çarpın çizge temelli yinelemeli alıcının bit-hata-olasılığı analizi incelenmiştir. Simulasyon sonuçları sunulan algoritmanın kanal bilgisini kullanarak MRC algoritmasına yakın bir performans sergilediğini ve performansının yinelemesiz ML algoritmasını geçtiğini göstermektedir.

GSIR'ın performansı deęişik örnek sembol araklıęı, kullanıcı sayısı, alıcı anten sayısı, kod oranı ve kümelerde algoritmaya genel bir bakış açısı oluşturmak için incelenmiştir. Ayrıca kanal kestirim performansı, GSIR kanal bilgisine sahip olduğu durumla karşılaştırılarak analiz edilmiştir. LDPC kod çözücü GSIR ile birlikte kullanılarak toplam performans arttırılmıştır.

Anahtar Kelimeler: MIMO-OFDM, çarpan çizge, Gauss mesaj iletimi, kanal kestirimi, yinelemeli alıcı, sönümlenmeli kanallar, bit-hata-olasılıęı analizi

To my family

ACKNOWLEDGMENTS

First, I would like to thank my supervisor Ali Özgür Yılmaz, who helped and guided me continuously despite his busy schedule.

I am also grateful to my colleagues especially Erkan Ersin Yıldırım who helped me when I had difficulty in studying. I thank my sister in-law İpek Kıvanç who helped me when I needed it most.

I thank my family, my sister Seçil Tekin and my mother Hayal Tekin notably my father Mehmet Tekin who supported me throughout my education and also encouraged me for Master of Science Degree.

Special thanks to my love and my wife Pınar Tekin and my daughter Derin Tekin; together they bring me happiness with their presence.

TABLE OF CONTENTS

ABSTRACT	v
ÖZ	vii
ACKNOWLEDGMENTS	x
TABLE OF CONTENTS	xi
LIST OF TABLES	xiv
LIST OF FIGURES	xv
LIST OF ABBREVIATIONS	xvii
CHAPTERS	
1 INTRODUCTION	1
2 THE FACTOR GRAPH APPROACH TO MIMO-OFDM	5
2.1 Multiple-Input Multiple-Output Transmission	5
2.1.1 MIMO Channel Model	6
2.1.2 Multiplexing Gain in MIMO	7
2.2 Orthogonal Frequency Division Multiplexing	8
2.2.1 Cyclic Prefix	10
2.2.2 OFDM Modulation	11

2.3	Factor Graphs	11
2.3.1	Sum-Product Message Passing Algorithm	15
2.3.2	Factor Graphs in Coding Theory	16
2.4	Graph-Based Representation of a MIMO-OFDM System . . .	18
3	GRAPH BASED SOFT-ITERATIVE RECEIVER	21
3.1	Channel Model	21
3.2	Transmitter and Receiver Structure	23
3.3	Training Symbols	25
3.4	Soft Channel Estimation	27
3.5	Soft Symbol Estimation	28
3.6	Information Exchange at Coefficient Nodes	29
3.7	Soft Data Detection	32
4	SIMULATION RESULTS	35
4.1	BER Performance of GSIR versus Non-iterative ML and MRC	36
4.2	BER Performance versus Number of Iterations	37
4.3	Channel Estimation versus Number of Iterations	39
4.4	BER Performance of GSIR with Different Training Spacing .	40
4.5	BER Performance of GSIR for Different Channel Models . .	40
4.6	BER Performance of GSIR with Different Number of Users and Receive Antennas	41
4.7	BER performance of GSIR with Different Code Rates	42
4.8	BER performance of GSIR with Different Constellations . .	44

4.9	BER performance of GSIR with Different Number of Users .	44
4.10	BER Performance of GSIR in Combination with LDPC . . .	45
4.11	BER Performance of GSIR in Combination with LDPC for Different Number of Users	46
5	CONCLUSION AND FUTURE WORKS	49
	REFERENCES	51

LIST OF TABLES

TABLES

LIST OF FIGURES

FIGURES

Figure 2.1	MIMO channel	6
Figure 2.2	Parallel decomposition of MIMO channel	9
Figure 2.3	Cyclic prefix of length μ	10
Figure 2.4	Transmitter and receiver structure of OFDM	12
Figure 2.5	An example of a factor graph	13
Figure 2.6	The factor graph of a system with two AWGN channels	14
Figure 2.7	Factor graph of a LDPC code	17
Figure 2.8	Factor graph of a RA code	18
Figure 2.9	The factor graph structure of a 2×2 MIMO-OFDM system	19
Figure 3.1	Multiuser MIMO channel model	21
Figure 3.2	Block diagram of transmitters and receiver	23
Figure 3.3	Factor graph structure of the GSIR process	24
Figure 3.4	Connections of the channel coefficients on the factor graph	25
Figure 3.5	Training grid of a multiuser MIMO-OFDM system	26
Figure 3.6	Message passing at frequency domain	31
Figure 3.7	Message exchange at a coefficient node	32
Figure 3.8	Extrinsic message exchange at a cloning node	33
Figure 4.1	BER performance of GSIR versus other algorithms	37
Figure 4.2	BER performance of 8×8 GSIR versus number of iterations	38

Figure 4.3	Channel estimation versus number of iterations	39
Figure 4.4	BER performance of GSIR with different training spacing	40
Figure 4.5	BER performance of GSIR for different channel modes	41
Figure 4.6	BER performance of GSIR with different number of users and receive antennas	42
Figure 4.7	BER performance of GSIR with different code rates	43
Figure 4.8	BER performance of GSIR with different constellations	44
Figure 4.9	BER performance of GSIR with different number of users	45
Figure 4.10	BER performance of GSIR in combination with LDPC	46
Figure 4.11	BER performance of GSIR in combination with LDPC for different number of users	47

LIST OF ABBREVIATIONS

AWGN	Additive White Gaussian Noise
BER	Bit-Error-Rate
BPSK	Binary Phase Shift Keying
CSI	Channel State Information
FFT	Fast Fourier Transform
GSIR	Graph-Based Soft Iterative Receiver
ICI	Inter-Carrier Interference
ISI	Inter-Symbol Interference
LDPC	Low-Density-Parity-Check
LLR	Log-likelihood Ratio
MAP	Maximum a Posteriori
MIMO	Multiple Input Multiple Output
ML	Maximum Likelihood
MRC	Maximum-Ratio-Combining
OFDM	Orthogonal Frequency Division Multiplexing
PAPR	Peak to Average Power Ratio
PCSI	Perfect Channel State Information
QAM	Quadrature Amplitude Modulation
RC	Repetition Code
SNR	Signal-to-Noise Ratio

CHAPTER 1

INTRODUCTION

Multiple-input multiple-output (MIMO) transmission in combination with orthogonal frequency division multiplexing (OFDM) is a key technology that satisfies the high throughput demands of next generation wireless systems [17],[16]. Also an interest in large-scale multiuser MIMO-OFDM systems have emerged with the increasing number of users in a wireless communication system. The space-division multiple access (SDMA) method using MIMO poses an alternative for multiuser systems with ten to hundred of users [20].

Channel knowledge at the receiver is an indispensable feature for new generation wireless systems. Channel state information (CSI), which involves channel responses, is obtained by using training symbols in order to enable high-quality detection and estimation. Training symbols, also called pilot signals [2], is known at the receiver and placed into a MIMO-OFDM frame to get more reliable CSI. Accuracy of CSI has an important role for system performance. While MIMO-OFDM provides high spectral efficiency, complexity and training overhead increases with the number of users. Especially the training overhead limits the number of permitted users, which bounds the spectral efficiency.

Graphical models are very effective techniques applied in many engineering problems. Factor Graphs are graphical models utilized in many areas such as coding, signal processing, machine learning, pattern recognition and statistics [9]. It is quite practical to design iterative algorithms with factor graphs especially in detection and estimation problems which involve many variables [10].

In conventional ML and MAP estimators, complexity increases exponentially with the modulation order and the number of users. Recently, there has been growing interest in suboptimal iterative expectation maximization algorithms [22], [21] that reduce receiver complexity.

Large-scale multiuser MIMO systems have attracted significant interests in recent years [11],[14], [5]. Reducing the complexity in systems with ten to hundred receive antennas and users has become a main issue for next generation multiuser wireless systems [15], [20].

Iterative graph-based receivers offer a low complexity framework for joint estimation and detection [19]. The belief propagation algorithm has been used for SISO/MIMO detection in [6]. A receiver that performs channel estimation and data detection over OFDM systems using belief propagation is proposed for a SISO system in [13] and for a MIMO system in [23]. Also accounting for the correlation between channel coefficients, soft channel estimation and soft data detection are applied for MIMO-OFDM systems [7] which we base our study. In another work [20], the authors propose graph-based iterative data detection for large-scale multiuser MIMO-OFDM systems.

The scope of this study is different from [7] and [20]. The work in [20] deals with complexity in large scale MIMO-OFDM systems with perfect channel knowledge at the receiver, while this study focuses on joint channel estimation and data detection for large scale multiuser MIMO-OFDM system without significant increase in training overhead and complexity. On the other hand, the receiver in [7] is capable of joint channel estimation and data detection with number of transmit antennas/users that are still limited due to training overhead and the receiver complexity is dependent on the modulation order. However in our proposed algorithm, channel estimation is feasible for numerous transmit antennas/users and high-order modulations can be used without significant increase in complexity.

In this study, a graph-based soft iterative algorithm is proposed for large scale multiuser MIMO-OFDM systems over time-varying frequency selective-channel. New transmitter and receiver structures are proposed for the users and the base-station in an uplink scenario. To make the receiver complexity less dependent on the modulation order, symbol estimates are utilized instead of symbol probabilities. All variables

are approximated as complex Gaussian and using the sum-product (belief propagation) algorithm on a graph, an approximate Gaussian message-passing algorithm is applied.

In addition, a new training structure is proposed which enable usage of a large number of transmit antennas/users. Different from [7], the ratio of training overhead is fixed and becomes independent of the number of users which alleviates the limitation on spectral efficiency.

In order to enhance performance, a new message-passing schedule is also introduced which reduces the effects of short-cycles occurring along iterations. Symbol and channel estimates are refined in each iteration by extrinsic information exchange. At the end of each iteration, symbol estimates are normalized with respect to the constellation for better detection performance.

Performance of the proposed graph-based soft iterative algorithm is studied through simulations. Channel estimation performance is investigated by comparing to the perfect channel state information case where channel coefficients are exactly known at the receiver. Non-iterative ML and MRC algorithms are applied and compared with the proposed algorithm. An LDPC encoder and decoder are added to the transmitter and receiver and a cascade structure is formed to enhance the total performance. System performance is tested over large-scale MIMO, or massive MIMO with tens to hundreds of users and receiver antennas (e.g. 32×32). The performance of multiuser MIMO-OFDM system with different constellations, code rates and number of users are presented to provide an overview for the proposed algorithm.

The thesis is organized as follows. In Chapter 2, the MIMO and OFDM techniques and the Factor Graphs are described to set up the factor graph approach for MIMO-OFDM. In Chapter 3, a new graph-based soft iterative receiver algorithm is proposed. Estimation, detection and message exchange algorithms are described. In Chapter 4, simulation results are presented. Finally, Chapter 5 concludes the study.

Throughout the study, following notations are used. Lowercase italic letters (e.g., x) denote scalars, bold lowercase letter denote vectors (e.g., \mathbf{x}) and matrices are represented by bold uppercase letters (e.g., \mathbf{X}). The superscripts $()^*$, $()^H$ denote conjugate

and Hermitian transpose and $E[\cdot]$ represents expectation operation. Parameters μ_x and σ_x^2 denote mean value and variance of a given random variable x .

CHAPTER 2

THE FACTOR GRAPH APPROACH TO MIMO-OFDM

In this chapter, the MIMO transmission and OFDM modulation techniques are described and their combination, namely MIMO-OFDM technique is explained. Modulation and demodulation method of OFDM are presented, advantages and disadvantages of OFDM are discussed. Finally, graph-based representation of a MIMO-OFDM system is indicated.

2.1 Multiple-Input Multiple-Output Transmission

In new generation wireless technologies, multiple-input multiple-output (MIMO) transmission in combination with orthogonal frequency division multiplexing (OFDM) is used as a common way to reach high data rates. It is a fact that frequency spectrum has become a limited resource with popularly used wireless systems and technologies. Using an assigned frequency band efficiently and increasing spectral efficiency is one of the main goals for new wireless technologies. MIMO satisfies these needs by providing spatial multiplexing gain and improving link reliability [1].

It is proved that different messages could be transmitted at the same time and in the same frequency band by using multiple antennas. It utilizes the fact that signals sent from different antennas arrive the receiver with differing channel gains. In this way, different data streams could be transmitted over multiple antennas [18].

Although multipath is seen as a destructive factor for the wireless channel, MIMO is a technology which benefits from the multipath propagation [3]. It has long been known

that beamforming could be utilized to attain array gain with channel knowledge at the transmitter. Also multiple receive antennas can be used for increasing diversity in order to combat fading and interference. However, the term MIMO usually means transmission of multiple data streams at the same time and frequency band to achieve spatial multiplexing and increasing capacity [1]. Unlike multiplexing in time and frequency domains, spectral efficiency can be increased by spatial multiplexing.

2.1.1 MIMO Channel Model

A narrowband communication system using N_t transmit and N_r receive antennas can be seen in Fig. 2.1 . Here $h_{n,m}$ denotes channel coefficient between m_{th} transmit antenna and n_{th} receive antenna.

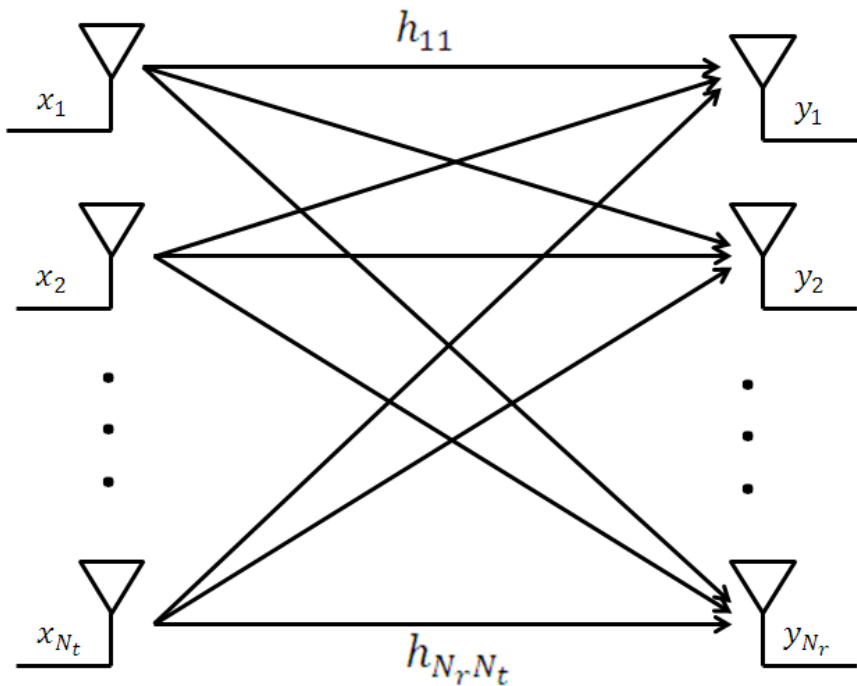


Figure 2.1: MIMO channel

This system can be modelled by the following discrete time model

$$\begin{bmatrix} y_1 \\ \vdots \\ y_{N_r} \end{bmatrix} = \begin{bmatrix} h_{1,1} & \dots & h_{1,N_t} \\ \vdots & \ddots & \vdots \\ h_{N_r,1} & \dots & h_{N_r,N_t} \end{bmatrix} \begin{bmatrix} x_1 \\ \vdots \\ x_{N_t} \end{bmatrix} + \begin{bmatrix} w_1 \\ \vdots \\ w_{N_r} \end{bmatrix} \quad (2.1)$$

or, in short by

$$\mathbf{y} = \mathbf{H}\mathbf{x} + \mathbf{w} \quad (2.2)$$

where \mathbf{x} represents the N_t dimensional transmitted symbol, \mathbf{y} symbolizes N_r dimensional received symbol and \mathbf{w} is the N_r dimensional zero-mean complex gaussian noise vector with covariance matrix $\sigma_n^2 \mathbf{I}_{N_r}$. The noise power at a receive antenna is denoted by σ_n^2 and equals to $N_0 B$.

For a given total transmit power P , the average SNR per antenna is calculated as $\rho = P/\sigma_n^2$ under unity channel gain when input symbols satisfy (2.3). In this calculation, it is usually assumed that the terms of the channel matrix \mathbf{H} have variance 1 and are independent. Equivalently, trace of the input covariance matrix must be equal to P as in (2.4)

$$\sum_{i=1}^{N_t} E[x_i x_i^*] = P, \quad (2.3)$$

$$\mathbf{R}_x = \mathbf{E}[\mathbf{x}\mathbf{x}^T], \text{Tr}(\mathbf{R}_x) = P. \quad (2.4)$$

2.1.2 Multiplexing Gain in MIMO

The use of multiple antennas at both the transmitter and receiver sides provides another performance gain called the multiplexing gain. A MIMO channel can be decomposed into a number R of parallel independent channels. Data rate can be roughly increased R times by multiplexing data onto these independent channels. This increase on data rate is referred to as multiplexing gain.

Let \mathbf{H} be an $N_r \times N_t$ MIMO channel gain matrix which is known both at the receiver and transmitter. For any matrix, its singular value decomposition (SVD) can be obtained as

$$\mathbf{H} = \mathbf{U}\mathbf{\Lambda}\mathbf{V}^H \quad (2.5)$$

where \mathbf{U} is an $N_r \times N_r$ and \mathbf{V} is an $N_t \times N_t$ unitary matrix. $\mathbf{\Lambda}$ is an $N_r \times N_t$ diagonal matrix which contains singular values λ_i of \mathbf{H} . The number of nonzero singular values is defined as the $rank(R)$ of the matrix. The rank of a matrix cannot be larger than the number of columns or rows, $R \leq \min(N_r, N_t)$. If the channel is rich scattering, the rank of the channel matrix is obtained by $R = \min(N_r, N_t)$ and it is a full rank matrix.

By transmitter precoding ($\mathbf{x} = \mathbf{V}\tilde{\mathbf{x}}$) and receiver shaping ($\mathbf{y} = \mathbf{U}^H\tilde{\mathbf{y}}$), a MIMO channel can be separated into independent channels. The parallel decomposition of the matrix is obtained as [3]

$$\tilde{\mathbf{y}} = \mathbf{U}^H(\mathbf{H}\mathbf{x} + \mathbf{w}) \quad (2.6)$$

$$= \mathbf{U}^H(\mathbf{U}\mathbf{\Lambda}\mathbf{V}^H\mathbf{x} + \mathbf{w}) \quad (2.7)$$

$$= \mathbf{U}^H(\mathbf{U}\mathbf{\Lambda}\mathbf{V}^H\mathbf{V}\tilde{\mathbf{x}} + \mathbf{w}) \quad (2.8)$$

$$= \mathbf{U}^H\mathbf{U}\mathbf{\Lambda}\mathbf{V}^H\mathbf{V}\tilde{\mathbf{x}} + \mathbf{U}^H\mathbf{w} \quad (2.9)$$

$$= \mathbf{\Lambda}\tilde{\mathbf{x}} + \tilde{\mathbf{w}} \quad (2.10)$$

where $\tilde{\mathbf{w}}$ and \mathbf{w} are identically distributed vectors. Parallel channels obtained by parallel decomposition can be seen in the Fig. 2.2.

2.2 Orthogonal Frequency Division Multiplexing

Orthogonal frequency division multiplexing (OFDM) is a multicarrier modulation method used for encoding data onto orthogonal subchannels. Although multicarrier modulation was invented before, computational complexity hindered its widespread use. Improvement on low-complexity algorithms such as Fast Fourier Transform (FFT) brought to mind that multicarrier modulation can be used with these algorithms which are easy to implement [3]. In this way, OFDM was invented and became a widespread technology.

OFDM increases reliability of communication system by dividing a channel into closely spaced subchannels which are referred to as subcarriers . This adjustment

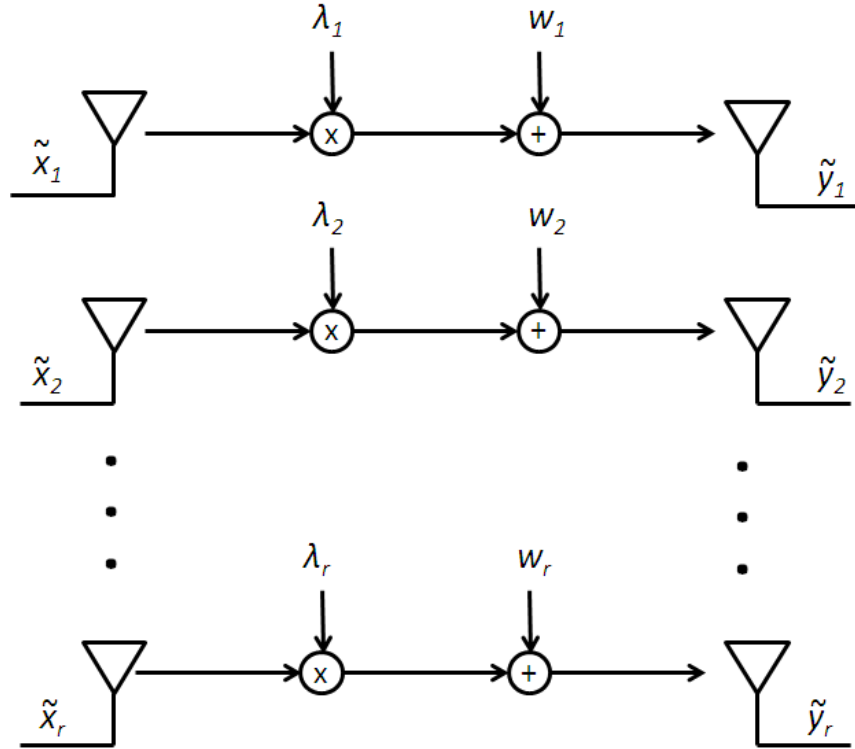


Figure 2.2: Parallel decomposition of MIMO channel

reduces the effect of Inter-Symbol Interference (ISI) which is one of the most corruptive factor for wireless channel [18]. The effects of ISI increases with the overlapping time of multipath signals and the desired signal. OFDM eliminates ISI by dividing high-bandwidth channel into numerous low-bandwidth channels. Thus symbol duration is increased and the proportion of multipath signals overlapping time is reduced.

Although OFDM has a lot of advantages, it suffers from several inherent problems. OFDM is sensitive to Doppler shift and frequency synchronization problems. Cyclic prefix or guard interval between OFDM symbols reduces the efficiency [1]. An OFDM transmission has a high peak-to-average-power ratio (PAPR). PAPR is increased by constructive addition of independent subcarrier phases and it is a huge problem for amplifiers at the transmitter side. Non-linearity of the amplifier can cause intermodulation which may increase the noise floor, create inter-carrier interference (ICI) and out-of-band radiation. Operation in the non-linear region is avoided by backing-off at the expense of reduced average transmitted power.

2.2.1 Cyclic Prefix

Cyclic Prefix is a data block which is transmitted during guard interval time and it is a copy of the last part of the OFDM symbol. At the receiver side, cyclic prefix allows taking circular convolution of the received samples which eliminates the ISI between transmitted symbols.

Cyclic prefix can be defined as $(x[N - \mu], \dots, x[N - 1])$ where the input sequence is $x[n] = (x[0], \dots, x[N - 1])$, N is the length of the sequence, $\mu + 1$ is the length of channel impulse response $h[n] = (h[0], \dots, h[\mu])$. The number of the taps $\mu + 1$ can be calculated by dividing maximum delay spread (T_m) to sampling time (T_s). Output sequence can be defined as $\tilde{x}[n] = (x[N - \mu], \dots, x[N - 1], x[0], \dots, x[N - 1])$ of length $N + \mu$ and shown in Fig. 2.3.

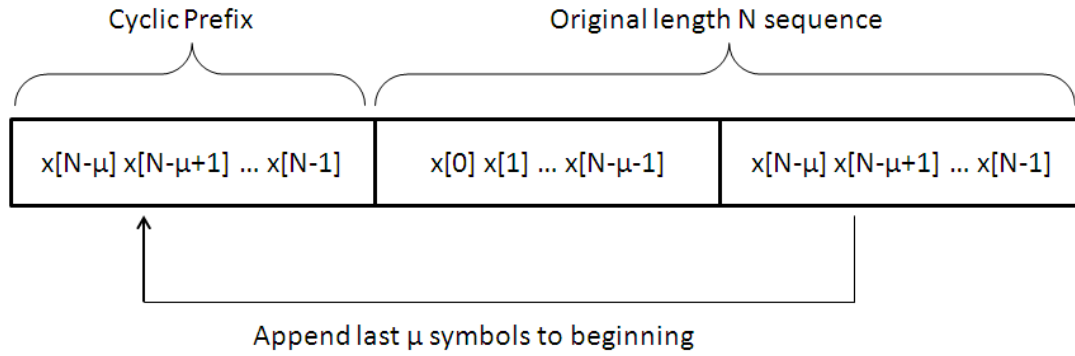


Figure 2.3: Cyclic prefix of length μ

Consider a output sequence of length $N + \mu$, the last N sample of the output can be calculated in the absence of noise as

$$\begin{aligned}
 y[n] &= \tilde{x}[n] * h[n] \\
 &= \sum_{k=0}^{\mu-1} h[k] \tilde{x}[n - k] \\
 &= \sum_{k=0}^{\mu-1} h[k] x[n - k]_N \\
 &= x[n] \otimes h[n]
 \end{aligned} \tag{2.11}$$

where \otimes denotes circular convolution which yields $Y[i] = X[i]H[i]$ in the frequency

domain. The input symbol can be detected by using (2.12) for a known channel impulse response.

$$X[i] = Y[i]/H[i] = DFT(y[n])/DFT(h(n)) \quad (2.12)$$

2.2.2 OFDM Modulation

The implementation of OFDM is shown in Fig. 2.4. The input data stream is modulated by a modulator, and complex symbol stream $X[0], X[1], \dots, X[N - 1]$ are obtained. These complex symbols are transformed to N parallel symbols by serial-to-parallel converter. Symbols are passed from frequency domain to time domain by the IFFT process. After adding CP, these discrete time samples are ordered by parallel-to-serial converter and the continuous time signal is constructed using digital to analog converters. Finally, the real and imaginary parts of the signal are upconverted to a carrier frequency.

The inverse of the same process is applied at the receiver. First, the signal is down-converted to baseband and filtered to remove high frequency components. The continuous time signal is transformed to discrete time samples by analog to digital converters. After removing Cyclic Prefix, N parallel symbols are obtained by serial-to-parallel converters. Symbols are passed from time domain to frequency domain by FFT process. Parallel symbol streams are converted to serial complex stream $\tilde{X}[0], \tilde{X}[1], \dots, \tilde{X}[N - 1]$ and demodulated to obtain desired data.

2.3 Factor Graphs

Graphical models are very effective representations with wide use in many disciplines. Factor Graphs are graphical models utilized in many areas such as coding, signal processing and statistics. It is more practical to design algorithms especially in detection and estimation problems which involve many variables [10].

A Factor-Graph is a bipartite graph that represents factorization of a function. Nodes constituting the factor-graph, are divided into two sets. These disjoint sets are named

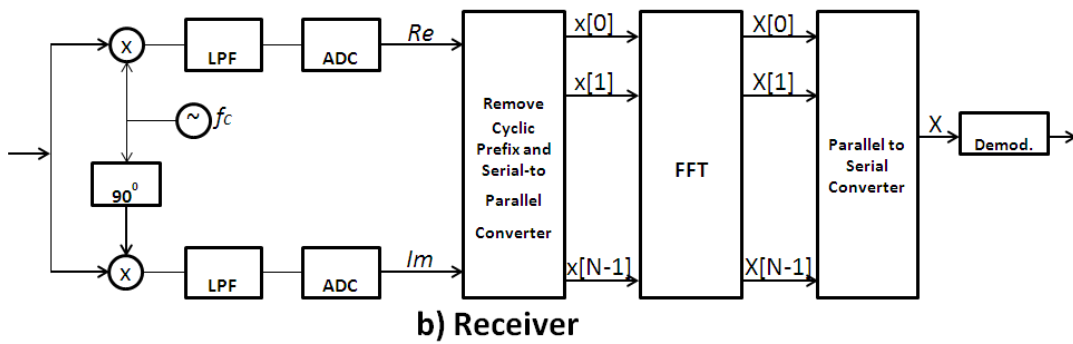
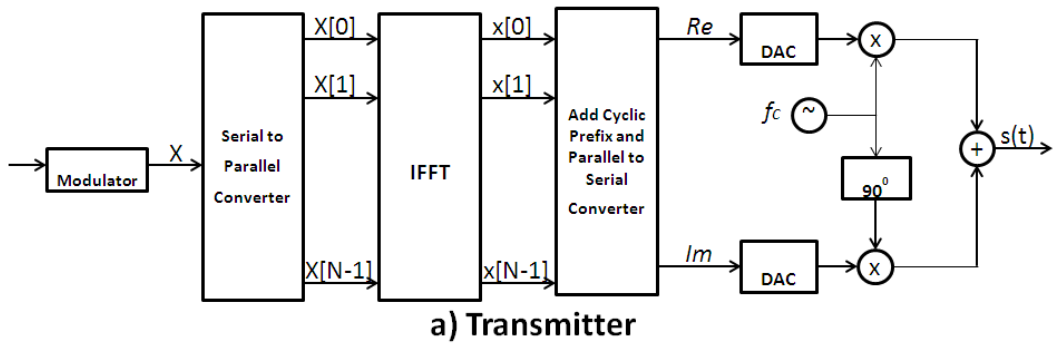


Figure 2.4: Transmitter and receiver structure of OFDM

as set of factor nodes and set of variable nodes. Every variable node must be connected to a factor node, but the connection between nodes in the same set is forbidden. These connections are also called as edges.

Factorization of a function can be modeled as follows

$$f(X_1, X_2, \dots, X_n) = \prod_{i=1}^m f_i(S_i) \quad (2.13)$$

where X_i 's are variable nodes, f_i 's are factor nodes, $S_i \subseteq \{X_1, X_2, \dots, X_n\}$, m is the number of factor nodes and n is the number of variable nodes. A factor graph can be represented as $G(F, X, E)$ which is a structure consisted of factors (F), variables (X) and edges (E).

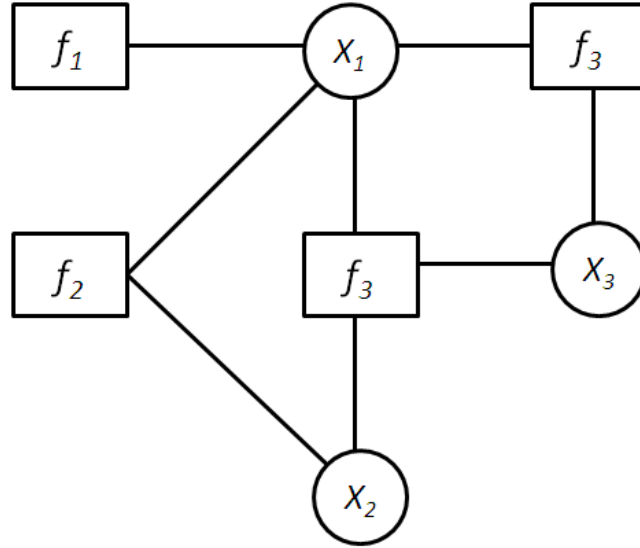


Figure 2.5: An example of a factor graph

Consider a function factored as follows

$$f(X_1, X_2, X_3) = f_1(X_1)f_2(X_1, X_2)f_3(X_1, X_2, X_3)f_4(X_1, X_3) \quad (2.14)$$

connection between f_1 and X_1 on a factor graph means that f_1 is a function of variable x_1 . The factorization in (2.14) corresponds to the factor graph in Fig. 2.5.

Using message passing algorithms like the sum-product algorithm and the max-product algorithm, certain characteristics of a factored function can be computed through the use of a factor graph [10]. In particular, marginal distributions of variables can be efficiently obtained by a factor graph combined with a suitable message passing algorithm.

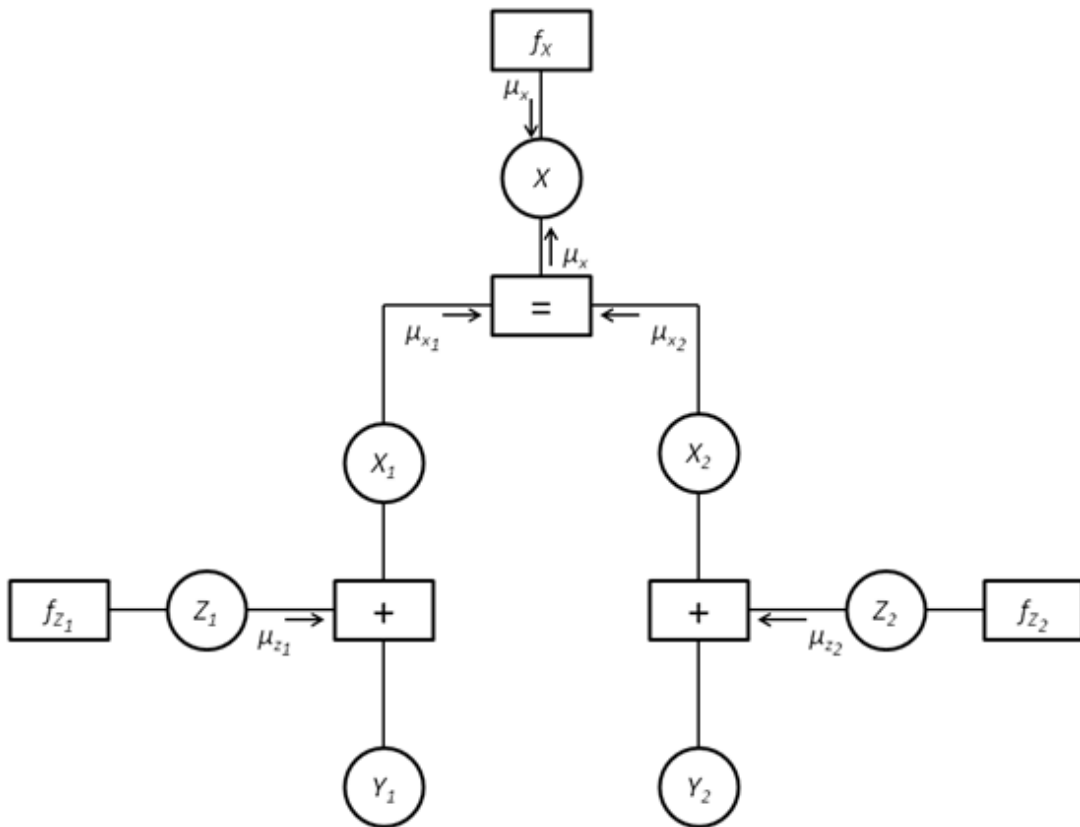


Figure 2.6: The factor graph of a system with two AWGN channels

As an example, a factor graph for a system that has two AWGN channels is depicted in Fig. 2.6. The symbol x is transmitted through two independent AWGN channels, z_1 and z_2 are gaussian noises, y_1 and y_2 are two independent observations. Factorization of the given system and equivalents of the factors are given below.

$$\begin{aligned}
f(x, x_1, x_2, z_1, z_2, y_1, y_2) &= \\
& p(x)p(z_1)p(z_2)f_=(x, x_1, x_2)f_+(x_1, z_1, y_1)f_+(x_2, z_2, y_2) \\
f_=(x, x_1, x_2) &= \delta(x - x_1)\delta(x - x_2) \\
f_+(x_1, y_1, z_1) &= \delta(x_1 + z_1 - y_1) \\
f_+(x_2, y_2, z_2) &= \delta(x_2 + z_2 - y_2)
\end{aligned} \tag{2.15}$$

$$\begin{aligned}
f(x, x_1, x_2, z_1, z_2, y_1, y_2) &= \\
& p(x)p(z_1)p(z_2)\delta(x - x_1)\delta(x - x_2)\delta(x_1 + z_1 - y_1)\delta(x_2 + z_2 - y_2)
\end{aligned}$$

Factor $\delta(x - x_1)\delta(x - x_2)$ represented by $=$ enforces variables x_1, x_2 to be equal to x and factor $\delta(x_n + z_n - y_n)$ represented by $+$ enforces $x_n + z_n = y_n$.

2.3.1 Sum-Product Message Passing Algorithm

The sum-product message passing, also known as belief propagation, is a message passing algorithm which provides calculation of marginal distributions on graphical models. Belief propagation is utilized in many topics especially in information theory. LDPC and turbo codes are the main applications on which the sum-product algorithm is successfully applied [10].

If $f(x_1, x_2, \dots, x_n)$ is a global function of discrete random variables, then the marginal function of X_k is computed by using the sum-product rule as

$$f(x_k) = \sum_{\mathbf{x}' \setminus x_k} f(\mathbf{x}') \tag{2.16}$$

where $\mathbf{x}' \setminus x_k$ denotes the set of discrete random variables X_1, X_2, \dots, X_n except X_k and $f(x_k)$ gives the probability distribution of X_k .

In the factor graph given in Fig. 2.6, a posteriori probability function of X for given observations y_1, y_2 can be calculated as

$$\begin{aligned} f(x|y_1, y_2) &\propto f(x, y_1, y_2) \\ &= \overrightarrow{\mu_X}(x) \overleftarrow{\mu_X}(x) \end{aligned} \quad (2.17)$$

where $\overrightarrow{\mu_X}(x)$ is the message that flows in the displayed \rightarrow direction and $\overleftarrow{\mu_X}(x)$ is the message that flows in the opposite way. Equalization for flowing messages are given as

$$\overrightarrow{\mu_X}(x) = f_X(x) \quad (2.18)$$

and messages sent from variable nodes X_1 and X_2 are found and then combined as

$$\overleftarrow{\mu_{X_1}}(x_1) = \int_{z_1} \delta(x_1 + z_1 - y_1) \overrightarrow{\mu_{Z_1}}(z_1) dz_1 \quad (2.19)$$

$$= \overrightarrow{\mu_{Z_1}}(y_1 - x_1) \quad (2.20)$$

$$= f_{Z_1}(y_1 - x - 1) \quad (2.21)$$

$$\overleftarrow{\mu_{X_2}}(x_2) = \int_{z_2} \delta(x_2 + z_2 - y_2) \overrightarrow{\mu_{Z_2}}(z_2) dz_2 \quad (2.22)$$

$$= \overrightarrow{\mu_{Z_2}}(y_2 - x_2) \quad (2.23)$$

$$= f_{Z_2}(y_2 - x_2) \quad (2.24)$$

$$\overleftarrow{\mu_X}(x) = \int_{x_1} \int_{x_2} \delta(x - x_1) \delta(x - x_2) \overleftarrow{\mu_{X_1}}(x_1) \overleftarrow{\mu_{X_2}}(x_2) dx_1 dx_2 \quad (2.25)$$

$$= \overleftarrow{\mu_{X_1}}(x) \overleftarrow{\mu_{X_2}}(x) \quad (2.26)$$

$$= f_{Z_1}(y_1 - x) f_{Z_2}(y_2 - x) \quad (2.27)$$

finally, probability function of X is calculated by using (2.17)

$$f(x|y_1, y_2) = f_X(x) f_{Z_1}(y_1 - x) f_{Z_2}(y_2 - x) \quad (2.28)$$

2.3.2 Factor Graphs in Coding Theory

Coding theory is one of the main areas where factor graphs are utilized. Factor graphs offer low complexity iterative receiver structures for forward error correction codes.

A factor graph structure for channel estimation and LDPC decoding is proposed in [12].

Message passing over factor graph can be allowed by using the sum-product algorithm [9] and soft information of the coded bits are exploited to obtain information bits. As an example, the factor graph structure of an LDPC code is depicted in Fig. 2.7 and factor graph of a repeat accumulate (RA) code is given in Fig. 2.8. LLR of the bits, which provide soft information, are exchanged in each iteration.

LLRs at the check nodes represented by \oplus are calculated as

$$b_3 = b_2 \oplus b_1$$

$$LLR_{b_3} = 2 \tanh^{-1}(\tanh(LLR_{b_1}/2) \tanh(LLR_{b_2}/2))$$
(2.29)

and LLRs at the cloning nodes represented by $=$ are calculated as

$$b_3 = b_2 = b_1$$

$$LLR_{b_3} = LLR_{b_1} + LLR_{b_2}$$
(2.30)

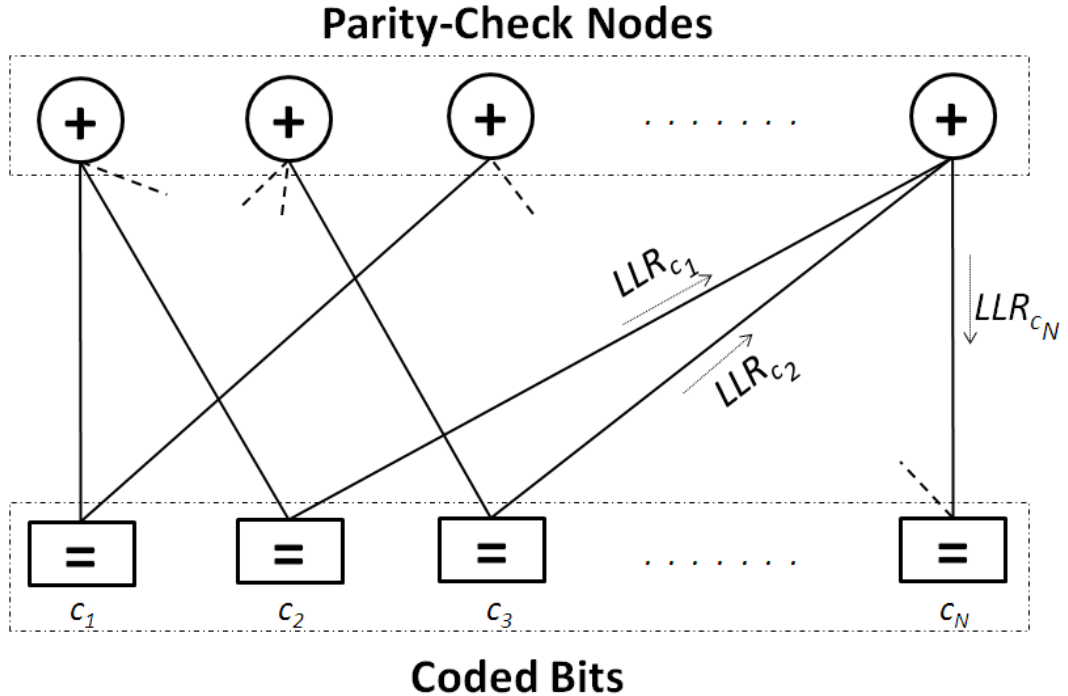


Figure 2.7: Factor graph of a LDPC code

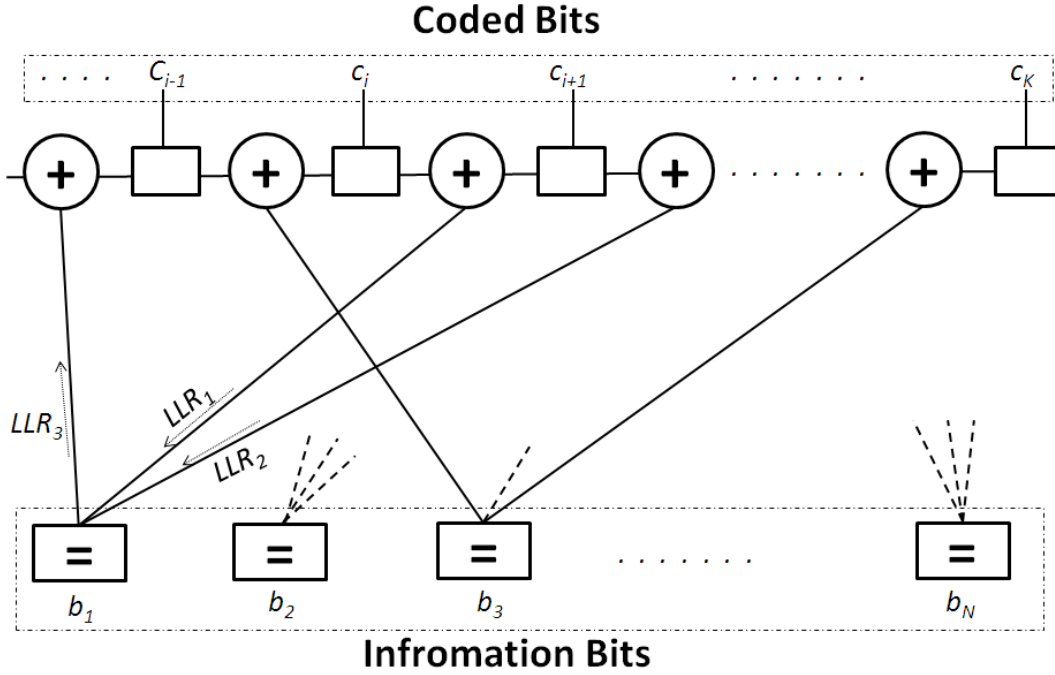


Figure 2.8: Factor graph of a RA code

2.4 Graph-Based Representation of a MIMO-OFDM System

MIMO-OFDM is a transmission and multiplexing technique that combines advantages of MIMO transmission and OFDM. After removing cyclic prefix and taking DFT of the received samples, a MIMO-OFDM system can be modeled in frequency domain as in (2.31), where i is the subcarrier index

$$Y_n(i) = \sum_{m=1}^M X_m(i) H_{n,m}(i) + Z_n(i). \quad (2.31)$$

The factor graph structure of a 2×2 MIMO-OFDM system for a given subcarrier is illustrated in Fig. 2.9 where observations Y_n and channel coefficients $H_{n,m}$ are known. The probability mass function of symbol variables X_1 and X_2 can be calculated by using the sum-product algorithm as in (2.17)

$$f(X_1, X_2 | H_{n,m}, Y_n) = \overrightarrow{\mu}_{X_1}(X_1) \overleftarrow{\mu}_{X_1}(X_1) \quad (2.32)$$

$$(2.33)$$

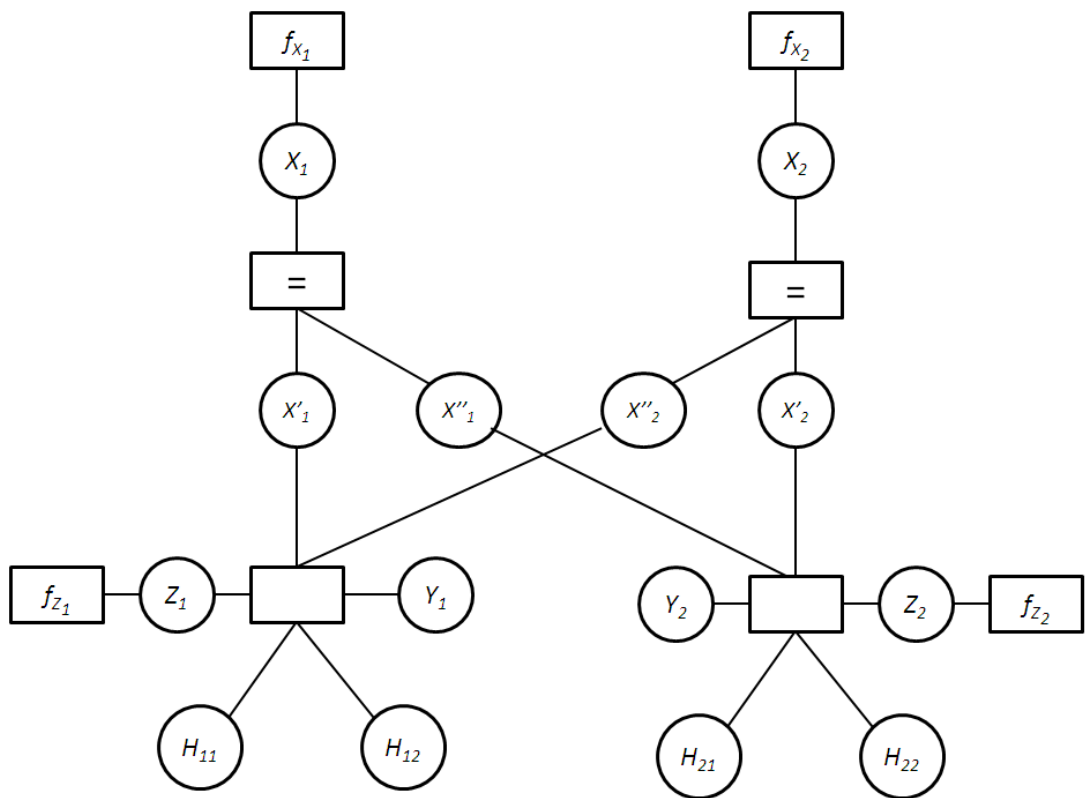


Figure 2.9: The factor graph structure of a 2×2 MIMO-OFDM system

and received messages are calculated by

$$\overrightarrow{\mu}_{X_1}(X_1) = f_{X_1}(X_1) \quad (2.34)$$

$$\overleftarrow{\mu}_{X_1}(X_1) = f_{X_2}(X_2)f_{Z_1}(Y_1 - \sum_{i=1}^2 H_{1,i}X_i)f_{Z_2}(Y_2 - \sum_{i=1}^2 H_{2,i}X_i) \quad (2.35)$$

$$(2.36)$$

finally we have

$$f(X_1, X_2 | H_{n,m}, Y_n) = f_{X_1}(X_1)f_{X_2}(X_2)f_{Z_1}(Y_1 - \sum_{i=1}^2 H_{1,i}X_i)f_{Z_2}(Y_2 - \sum_{i=1}^2 H_{2,i}X_i) \quad (2.37)$$

CHAPTER 3

GRAPH BASED SOFT-ITERATIVE RECEIVER

In this chapter, a channel model over which the proposed multiuser graph based soft-iterative receiver (GSIR) operates is first defined. The transmitter structure, the receiver structure and associated factor graph are described.

3.1 Channel Model

The uplink of a multiuser MIMO-OFDM system with M users and one base-station is considered. Each user has only one transmit antenna and the base-station has N receiver antennas. The channel model of the system is illustrated in Fig. 3.1.

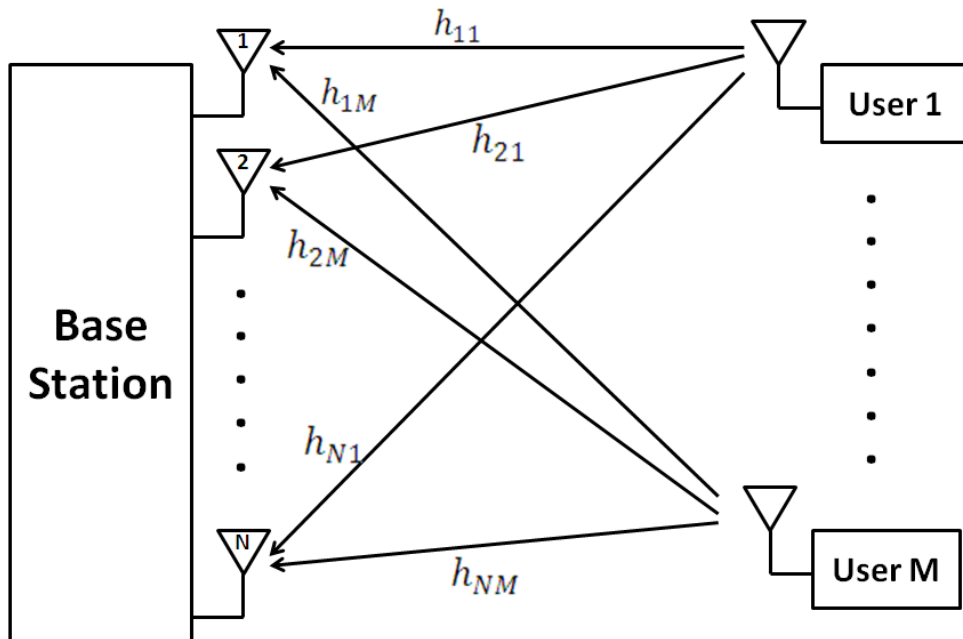


Figure 3.1: Multiuser MIMO channel model

The MIMO-OFDM frame consists of L OFDM subcarriers and K OFDM symbols. After OFDM demodulation, discrete time model of the channel can be formed as [7].

$$\begin{aligned}
y_n(l, k) &= \sum_{i=1}^M h_{n,i}(l, k)x_i(l, k) + w_n(l, k) \\
&= h_{n,m}(l, k)x_m(l, k) + \underbrace{\sum_{i=1, i \neq m}^M h_{n,i}(l, k)x_i(l, k)}_{\text{MAI}} + \underbrace{w_n(l, k)}_{\text{AWGN}}
\end{aligned} \tag{3.1}$$

where l and k represent the subcarrier and symbol indexes respectively, y_n is the received signal at the n th receive antenna, x_m is the transmitted signal from m th user. $h_{n,m}$ denotes channel coefficient between m th user's transmit antenna and n th receive antenna. Multi-Antenna Interference (MAI) consists of $(M - 1)$ signals from other users. Combined with the Gaussian noise term w_n , MAI corrupts the desired signal.

The total interference is called effective noise and consists of MAI and the AWGN term and denoted by $v_{n,m}(l, k)$

$$v_{n,m}(l, k) = \sum_{i=1, i \neq m}^M h_{n,i}(l, k)x_i(l, k) + w_n(l, k) \tag{3.2}$$

so that

$$y_n(l, k) = h_{n,m}(l, k)x_m(l, k) + v_{n,m}(l, k) \tag{3.3}$$

The channel coefficients are unit power, zero mean complex Gaussian variables $N_C(0, 1)$ and can be modeled as [4]

$$h_{n,m}(l, k) = \lim_{N_p \rightarrow \infty} \frac{1}{\sqrt{N_p}} \sum_{i=1}^{N_p} \exp(j(\theta_i + 2\pi f_{D,i}kT_s - 2\pi\tau_i lF)) \tag{3.4}$$

where OFDM symbol duration and OFDM subcarrier spacing are denoted by T_s and F . N_p is the number of the multipath components and assumed to be infinite. Random phase $\theta_i \in [0, 2\pi)$, Doppler frequency $f_{D,i} \in [-f_{D,max}, f_{D,max}]$ and propagation delay $\tau_i \in [0, \tau_{max}]$ are the other factors that affect multipath component.

Howbeit ,channel coefficients are correlated in the spatial domain in [4], whereas coefficients are assumed to be uncorrelated in the spatial domain in our channel model due to the mobility of users so that

$$\mathbf{E}[h_{n,i}^* h_{n,j}] = 0, \text{ for all } i \neq j. \quad (3.5)$$

3.2 Transmitter and Receiver Structure

Transmitter structures of the users and the receiver structure of the base station are illustrated in Fig.3.2, where Π represents the interleaver. The mapper performs the modulation operation. The modulated symbols are repeated and then interleaved by an interleaver known at the receiver. Then, training symbols are inserted to the frame and OFDM modulation is applied. Finally modulated symbols of the users are transmitted simultaneously over the MIMO channel.

As a channel code, repetition code is used but the only difference is instead of bits the symbols are repeated. Thus, message-passing between symbols is enabled which increases the performance of the receiver and decreases the complexity of the algorithm.

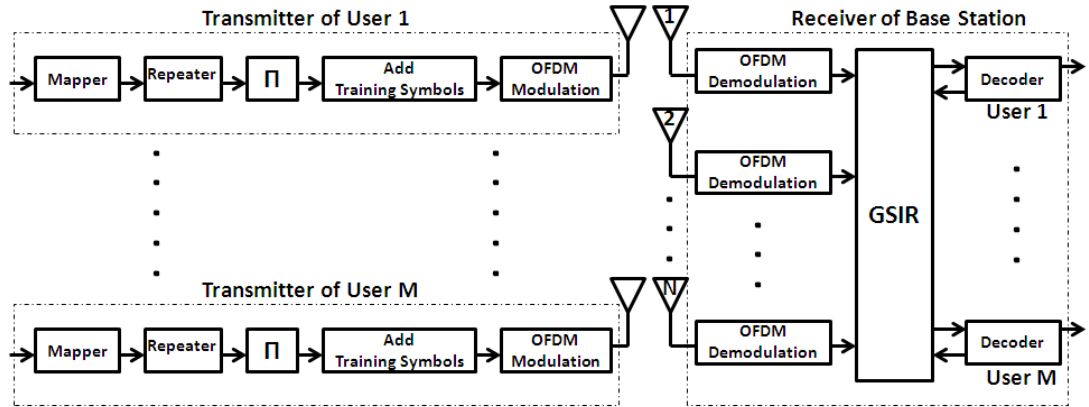


Figure 3.2: Block diagram of transmitters and receiver

At the receiver side, time domain samples received from each antenna are first converted to frequency domain by OFDM demodulation. GSIR utilizes the whole information in the frame to jointly perform channel estimation and data detection. The

information generated about symbols are passed to the channel decoder and extrinsic information are fed back to the GSIR to be used in subsequent iteration. Finally, the decoder makes a decision using the information refined throughout iterations.

Fig. 3.3 illustrates the factor graph structure of a Multiuser MIMO-OFDM system with 2 users, 2 receive antennas at the base station and connections of coefficients only in frequency domain. In Fig. 3.3 Cloning nodes ($=$), observation nodes (y), transfer nodes (Δ) are represented by rectangles and symbol nodes (x), coefficient nodes (h) are represented by circles. The parameters μ and σ^2 denote mean values and variances of the variables which provide soft information.

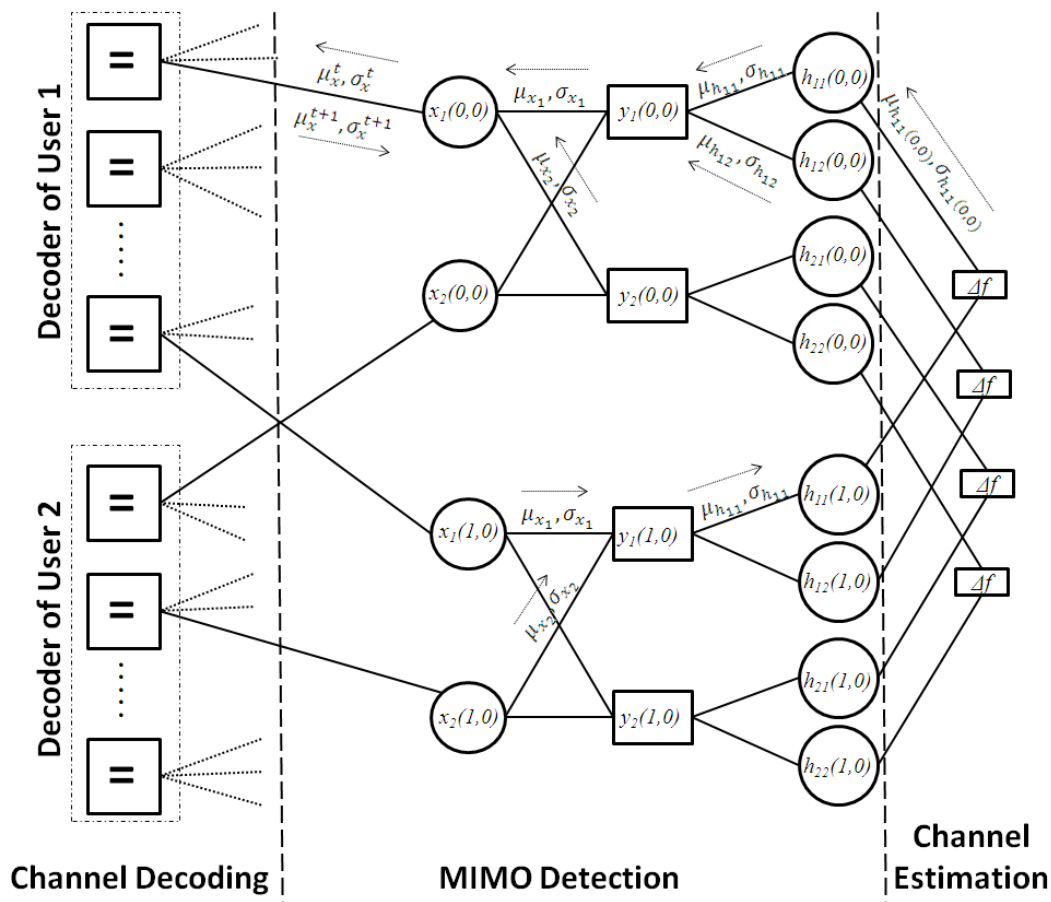


Figure 3.3: Factor graph structure of the GSIR process

Connections of the coefficient nodes on the factor graph are illustrated in Fig. 3.4. In time and frequency domain, transfer nodes enable connection between neighboring coefficient nodes.

A GSIR process can be summarized as

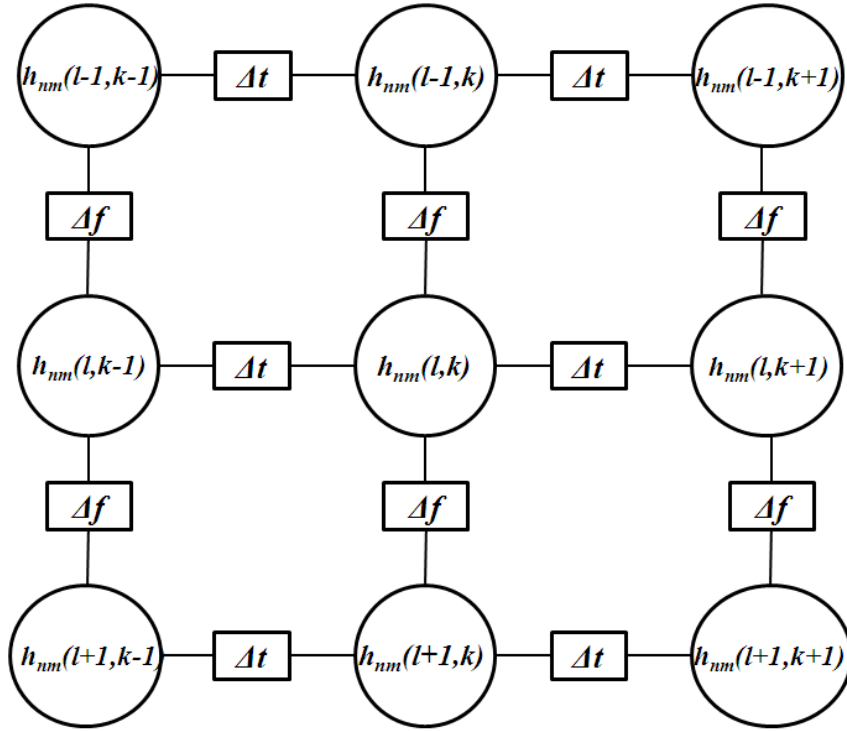


Figure 3.4: Connections of the channel coefficients on the factor graph

1. At first, channel estimation is applied so that mean values and variances of the channel coefficients are calculated by utilizing observations, previous channel estimates and soft information of the symbols.
2. Information exchange between coefficient nodes is utilized. Soft information of the channel coefficients are distributed to the frame by transfer nodes according to the message passing algorithm and coefficient nodes combine all incoming messages to update coefficient estimates.
3. Symbol estimation is applied by recalculating mean values and variances of the symbols with updated channel coefficient estimates.
4. Finally, updated symbol estimates are passed to the decoder for subsequent iterations.

3.3 Training Symbols

Training symbols are transmitted signals for providing channel information to the receiver. Training symbols of the users are independent from each other and known

exactly at the receiver side.

Training Symbols are placed in the frame according to Fig. 3.5. Training symbols are interspersed with period D_t in time domain and D_f in frequency domain. Different from [7], all users are transmitting their training symbols at the same positions in the frame so that wasted usage of bandwidth is prevented. Another advantage of this proposal is that the limitation of user or transmit antenna numbers due to the training overhead is eliminated.

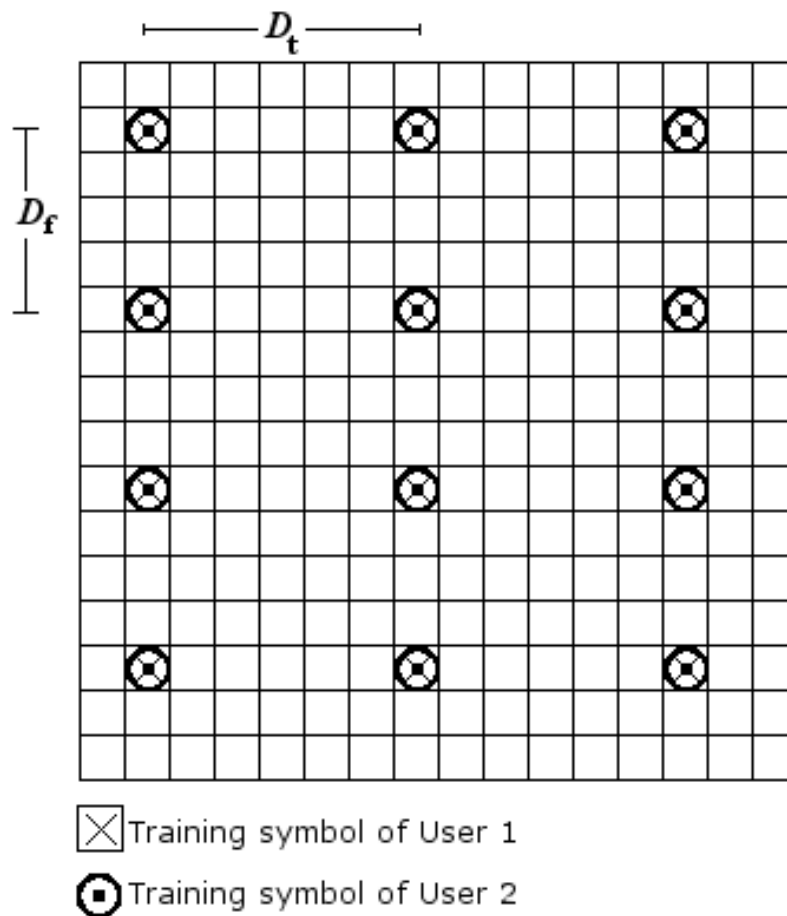


Figure 3.5: Training grid of a multiuser MIMO-OFDM system

At the training symbol positions, the receiver does not perform symbol estimation, however, channel estimation and information exchange are utilized. Since actual values of the training symbols are known, mean values of symbols are set to the known values and variances are taken to be zero. Initial channel estimation at a training symbol position is given in (3.6) where x_{tr_m} denotes training symbol of m_{th} user.

$$\begin{aligned}
y_n &= h_{n,m}x_{tr_m} + v_{n,m} \\
\mu_{h_{n,m}} &= \mathbf{E}[h_{n,m}|x_{tr_1}, \dots, x_{tr_M}, y_n] = \frac{y_n - \mu_{v_{n,m}}}{x_{tr_m}} \\
\mu_{v_{n,m}} &= \mathbf{E}\left[\sum_{i=1, i \neq m}^M h_{n,i}x_{tr_i} + w_n\right] \\
\mu_{v_{n,m}} &= \sum_{i=1, i \neq m}^M \underbrace{\mu_{h_{n,i}}}_{0} x_{tr_i} + \underbrace{\mu_{w_n}}_0 = 0 \\
\mu_{h_{n,m}} &= \frac{y_n}{x_{tr_m}}
\end{aligned} \tag{3.6}$$

At first iteration, mean values are taken to be zero and variances equal to 1 for all coefficients. It is sufficient for initial estimation at the training symbol position. Starting with training symbol positions, channel estimates get more accurate in each iteration.

The choice of training symbols affects the reliability of initial channel estimation. It is observed that training symbols which yield $\sum_i x_{tr_i} \approx 0$ achieve better performance.

3.4 Soft Channel Estimation

Channel estimation is a process applied in the observation nodes to calculate soft information of the channel coefficients. Previous channel estimates, observation and symbol estimates are exploited for the computation. All variables are assumed to be complex Gaussian which have a mean and a variance value. This facility also reduces the complexity of the proposed algorithm.

The mean value of the channel coefficient at a given position is approximated by

$$\mu_{h_{n,m}} = \mathbf{E}[h_{n,m}|x_m, y_n] \quad (3.7)$$

$$= \frac{y_n - \mu_{v_{n,m}}}{x_m} \quad (3.8)$$

$$\mu_{v_{n,m}} = \sum_{i \neq m} \mu_{h_{n,i}} \mu_{x_i} \quad (3.9)$$

$$\frac{1}{x_m} \approx \frac{\mu_{x_m}^*}{|\mu_{x_m}|^2 + \sigma_{x_m}^2} \quad (3.10)$$

$$\mu_{h_{n,m}} \approx \frac{(y_n - \sum_{i \neq m} \mu_{h_{n,i}} \mu_{x_i}) \mu_{x_m}^*}{|\mu_{x_m}|^2 + \sigma_{x_m}^2} \quad (3.11)$$

Approximation in (3.10) is utilized to estimate $1/x_m$ by using μ_{x_m} and $\sigma_{x_m}^2$. In each iteration, where $|x_m - \mu_{x_m}|$ and $\sigma_{x_m}^2$ is decreasing, this approximation gets more accurate. A Similar approximation is used to calculate the variance of the channel coefficient in (3.17).

$$\sigma_{h_{n,m}}^2 = \frac{\sigma_{v_{n,m}}^2}{|x_m|^2} \quad (3.12)$$

$$\sigma_{v_{n,m}}^2 = \sum_{i \neq m} \mathbf{E}[|h_{n,i} x_i|^2] - \sum_{i \neq m} |\mathbf{E}[h_{n,i} x_i]|^2 + \sigma_{w_n}^2 \quad (3.13)$$

$$\sigma_{v_{n,m}}^2 = \sum_{i \neq m} \mathbf{E}[|h_{n,i}|^2] \mathbf{E}[|x_i|^2] - \sum_{i \neq m} |\mathbf{E}[h_{n,i}]|^2 |\mathbf{E}[x_i]|^2 + \sigma_{w_n}^2 \quad (3.14)$$

$$\sigma_{v_{n,m}}^2 = \sum_{i \neq m} (|\mu_{h_{n,i}}|^2 + \sigma_{h_{n,i}}^2) (|\mu_{x_i}|^2 + \sigma_{x_i}^2) - \sum_{i \neq m} |\mu_{h_{n,i}}|^2 |\mu_{x_i}|^2 + \sigma_{w_n}^2 \quad (3.15)$$

$$\sigma_{v_{n,m}}^2 = \sum_{i \neq m} (|\mu_{h_{n,i}}|^2 \sigma_{x_i}^2 + |\mu_{x_i}|^2 \sigma_{h_{n,i}}^2 + \sigma_{h_{n,i}}^2 \sigma_{x_i}^2) + \sigma_{w_n}^2 \quad (3.16)$$

$$\frac{1}{|x_m|^2} \approx \frac{1}{|\mu_{x_m}|^2 + \sigma_{x_m}^2} \quad (3.17)$$

$$\sigma_{h_{n,m}}^2 \approx \frac{\sum_{i \neq m} (|\mu_{h_{n,i}}|^2 \sigma_{x_i}^2 + |\mu_{x_i}|^2 \sigma_{h_{n,i}}^2 + \sigma_{h_{n,i}}^2 \sigma_{x_i}^2) + \sigma_{w_n}^2}{|\mu_{x_m}|^2 + \sigma_{x_m}^2} \quad (3.18)$$

3.5 Soft Symbol Estimation

The task of symbol estimation is to calculate the mean and variance values of the transmitted symbols. Previous symbol estimates, updated channel estimates after message exchange and observations are utilized for the calculation.

In the first iteration, $\mu_x = 0$ and $\sigma_x^2 = 1$ for all symbol estimates. Estimations are refined in each iteration so that μ_{x_m} converges ideally to the symbol transmitted from m th user and $\sigma_{x_m}^2$ converges to zero.

$$\mu_{x_m} = \mathbf{E}[x_m | h_{n,m}, y_n] \quad (3.19)$$

$$= \frac{y_n - \mu_{v_{n,m}}}{h_{n,m}} \quad (3.20)$$

$$\frac{1}{h_{n,m}} \approx \frac{\mu_{h_{n,m}}^*}{|\mu_{h_{n,m}}|^2 + \sigma_{h_{n,m}}^2} \quad (3.21)$$

$$\mu_{x_m} \approx \frac{(y_n - \sum_{i \neq m} \mu_{h_{n,i}} \mu_{x_i}) \mu_{h_{n,m}}^*}{|\mu_{h_{n,m}}|^2 + \sigma_{h_{n,m}}^2} \quad (3.22)$$

Approximations in (3.19) and (3.23) are obtained in a similar way utilized to estimate channel coefficients.

$$\sigma_{x_m}^2 = \frac{\sigma_{v_{n,m}}^2}{|h_{n,m}|^2} \quad (3.23)$$

$$\frac{1}{|h_{n,m}|^2} \approx \frac{1}{|\mu_{h_{n,m}}|^2 + \sigma_{h_{n,m}}^2} \quad (3.24)$$

$$\sigma_{x_m}^2 \approx \frac{\sum_{i \neq m} (|\mu_{h_{n,i}}|^2 \sigma_{x_i}^2 + |\mu_{x_i}|^2 \sigma_{h_{n,i}}^2 + \sigma_{h_{n,i}}^2 \sigma_{x_i}^2) + \sigma_{w_n}^2}{|\mu_{h_{n,m}}|^2 + \sigma_{h_{n,m}}^2} \quad (3.25)$$

3.6 Information Exchange at Coefficient Nodes

Coefficient nodes are connected to each other for the purpose of exchanging their information so that accuracy of channel estimation could be improved. These connections are obtained by transfer nodes in time and frequency domains. Transfer nodes convert probability information of a coefficient node to probability information of its neighbor by using the correlation between them.

The deviation between two adjacent channel coefficients is denoted by Δ and approximated by a zero-mean complex Gaussian variable [7]. The variable h' represents the subsequent coefficient coming after h in a given domain so that

$$\Delta \sim N_C(0, \sigma_\Delta^2) \quad (3.26)$$

$$\Delta = h' - wh, \quad |w| = 1 \quad (3.27)$$

where w is called the tuning factor [7] which refers to the expected phase shift between coefficients. The variables w and Δ determine the correlation properties used in message exchange. At the transfer nodes, the mean and variance values of the adjacent coefficient h' are calculated as

$$\mu_{h'} = w\mu_h \quad (3.28)$$

$$\sigma_{h'}^2 = \sigma_h^2 + \sigma_\Delta^2 \quad (3.29)$$

The reliability of the information is decreased in each transfer node by adding σ_Δ^2 to the variance. The variance of the transfer node and the tuning factor can be calculated by using correlation function $\mathbf{E}[h^*h']$ as in (3.30) [7].

$$\begin{aligned} \sigma_\Delta^2 &= \mathbf{E}[|h' - wh|^2] \\ &= \underbrace{\mathbf{E}[|h'|^2]}_1 + \underbrace{\mathbf{E}[|h|^2]}_1 - \mathbf{E}[w^*h^*h'] - \mathbf{E}[whh'^*] \\ &= 2(1 - \text{Re}(w^*\mathbf{E}[h^*h'])) \quad (3.30) \\ w &= \arg \min_{|w|=1}(\sigma_\Delta^2) = \frac{\mathbf{E}[h^*h']}{|\mathbf{E}[h^*h']|} \\ \sigma_\Delta^2 &= 2(1 - |\mathbf{E}[h^*h']|) \end{aligned}$$

The correlation between adjacent coefficients in frequency domain for uniformly distributed power of multipaths is given by [7]

$$\mathbf{E}[h_{n,m}^*(l, k)h_{n,m}(l+1, k)] = \text{sinc}(\tau_{max}F)e^{-j(\pi\tau_{max}F)} \quad (3.31)$$

and correlation function between adjacent coefficients in time domain can be found

by

$$\mathbf{E}[h_{n,m}^*(l, k)h_{n,m}(l, k + 1)] = \text{sinc}(2f_{D,max}T_s) \quad (3.32)$$

By substituting (3.31) and (3.32) into (3.30), tuning factors and variances in the time and frequency domain turn out to be

$$w_f = e^{-j(\pi\tau_{max}F)}, \quad \sigma_{\Delta_f}^2 = \text{sinc}(\tau_{max}F) \quad (3.33)$$

$$w_t = 1, \quad \sigma_{\Delta_t}^2 = \text{sinc}(2f_{D,max}T_s) \quad (3.34)$$

Message-passing at a coefficient node in one direction of the frequency domain can be observed in Fig. 3.6. Message sent to a transfer node $(\vec{\mu}_{h(l,k)}, \vec{\sigma}_{h(l,k)}^2)$ is obtained by combining messages received from the observation node and the previous transfer node as in (3.35).

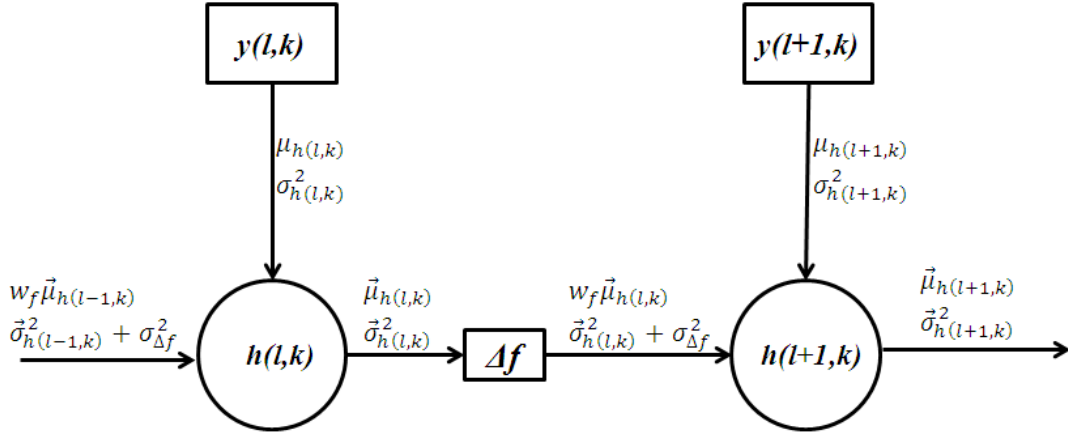


Figure 3.6: Message passing at frequency domain

In [7], after completion of message passing in two direction, incoming messages in one domain are combined. However in the proposed algorithms, all incoming messages in both domains are combined as illustrated in Fig. 3.7. It is observed that the performance is enhanced due to the mitigation of short cycles. Short cycles happen if a message which leaves a node, reaches the same node after travelling a short path. After combining messages, they are passed to the observation node and then utilized for symbol estimation.

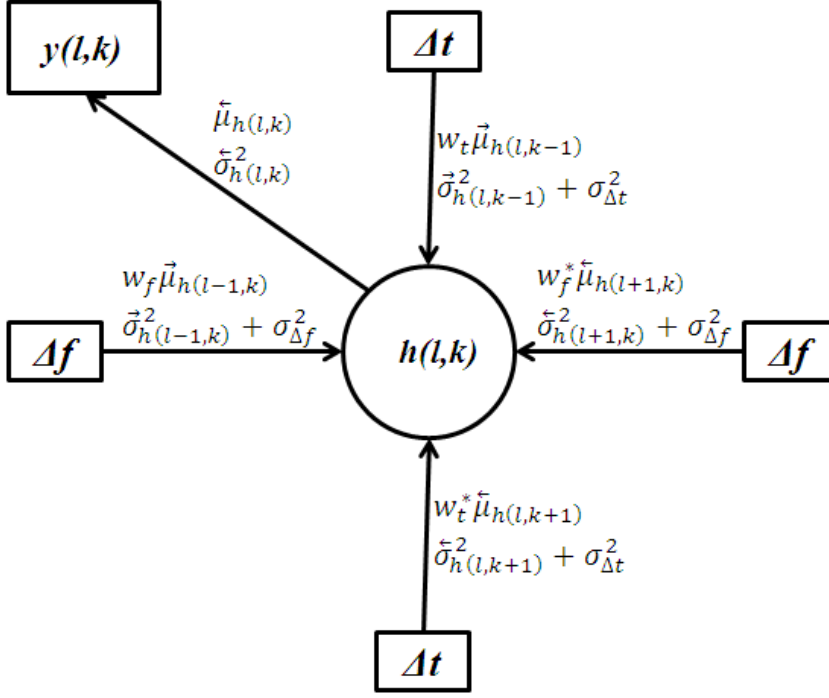


Figure 3.7: Message exchange at a coefficient node

Mean value μ_c and variance σ_c^2 of a combined message are calculated as in (3.35), where μ_i and σ_i^2 constitute the incoming message [7]

$$\mu_c = \frac{\sum_i \frac{\mu_i}{\sigma_i^2}}{\sum_i \frac{1}{\sigma_i^2}}, \quad \sigma_c^2 = \frac{1}{\sum_i \frac{1}{\sigma_i^2}}. \quad (3.35)$$

3.7 Soft Data Detection

Soft data detection is a process applied in the decoder. After symbol estimation, messages coming from different receiver antennas are combined as in (3.35) and passed to the decoder. The task of the decoder is to feed back extrinsic information throughout iterations and at the end make a decision by using combined messages coming from GSIR.

Extrinsic information exchange at a cloning node is illustrated in Fig. 3.8, where (l_r, k_r) denotes repeated symbol positions in the frame, t is the iteration number and R represents the number of the repeated symbols. To calculate extrinsic information of a node, messages from all symbol nodes except the node itself are combined as in

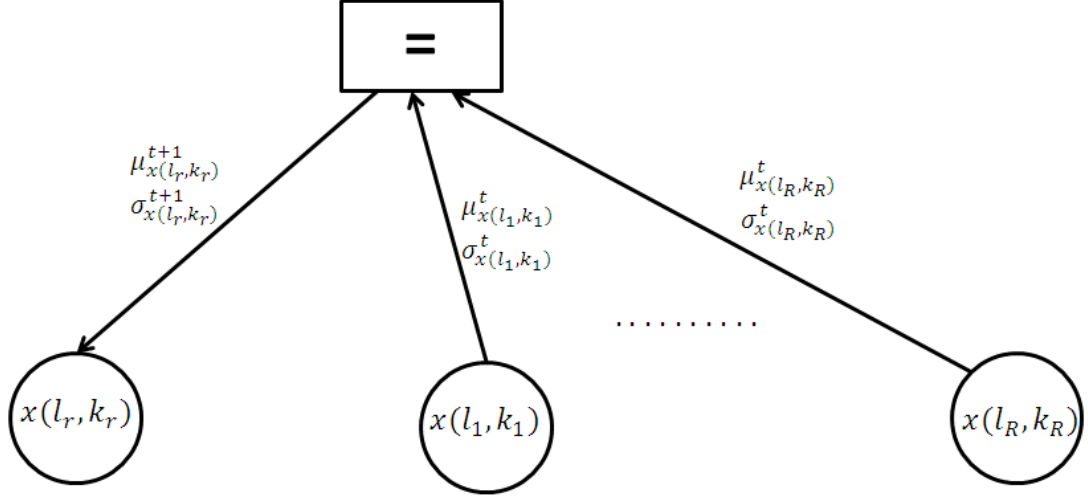


Figure 3.8: Extrinsic message exchange at a cloning node

(3.36).

$$\mu_{x(l_r, k_r)}^{t+1} = \frac{\sum_{i=1, i \neq r}^R \frac{\mu_{x(l_i, k_i)}^t}{\sigma_{x(l_i, k_i)}^{2t}}}{\sum_{i=1, i \neq r}^R \frac{1}{\sigma_{x(l_i, k_i)}^{2t}}}, \quad \sigma_{x(l_r, k_r)}^{2t+1} = \frac{1}{\sum_{i=1, i \neq r}^R \frac{1}{\sigma_{x(l_i, k_i)}^{2t}}} \quad (3.36)$$

It may happen that the symbol estimate is out of the constellation boundary. In that case, it is normalized in each iteration to prevent $|\mu_x| \gg 1$. A similar idea has been utilized in [20]. Normalization of symbol estimates is summarized in (3.37), where x_i represents the constellation points.

$$\hat{\mu}_x = \frac{\sum_i x_i e^{-\frac{|\mu_x - x_i|^2}{\sigma_x^2}}}{\sum_i e^{-\frac{|\mu_x - x_i|^2}{\sigma_x^2}}}, \quad \hat{\sigma}_x^2 = \frac{\sum_i |x_i|^2 e^{-\frac{|\mu_x - x_i|^2}{\sigma_x^2}}}{\sum_i e^{-\frac{|\mu_x - x_i|^2}{\sigma_x^2}}} - |\hat{\mu}_x|^2 \quad (3.37)$$

Finally, at the end of the last iteration, messages sent from repeated symbols are combined and the LLR of bits contained in symbol is approximated as

$$LLR(b_v) \approx \max_{x_i(b_v=0)} \left(-\frac{|x_i - \mu_x|^2}{\sigma_x^2} \right) - \max_{x_i(b_v=1)} \left(-\frac{|x_i - \mu_x|^2}{\sigma_x^2} \right) \quad (3.38)$$

where $x_i(b_v = 0)$ denotes the symbols that v_{th} bit is equal to zero.

CHAPTER 4

SIMULATION RESULTS

In this chapter, BER performance of the proposed algorithm is analyzed by means of Monte Carlo simulations for different training symbol spacing, number of users, number of receive antennas and code rates. Accuracy of channel estimation and data detection are examined in each iteration. GSIR with perfect channel knowledge is applied to compare the performance of channel estimations. An LDPC encoder and decoder are used in combination with GSIR to increase total performance.

The channel model in [4] is utilized to generate channel coefficients. Correlation matrices between channel coefficients in time and frequency domain are found by using (3.32) and (3.31). Channel coefficients are correlated in each domain as

$$\mathbf{h}' = \mathbf{h}\mathbf{R}_{\mathbf{h}}^{1/2} \quad (4.1)$$

where \mathbf{h} is independently generated channel coefficient vector with correlation matrix \mathbf{I} and the correlation matrix in the given domain is denoted by $\mathbf{R}_{\mathbf{h}}$. Normalized fading is taken to be 0.01 which yields $\tau_{max}F = 0.01$ and $f_{D,max}T_s = 0.01$. Channel model with uniformly distributed parameters $f_{D,max}$ and τ_{max} is used in all simulations except Fig.4.5.

System parameters subcarrier spacing, symbol duration and carrier frequency are taken to be $F = 15$ kHz, $T_s = 71.43\mu s$ and $f_c = 800$ MHz. For $f_{D,max}T_s = 0.01$, maximum Doppler frequency $f_{D,max}$ is equal to 140 Hz. By using $v_{max} = cf_{D,max}/f_c$, maximum velocity results in $v_{max} = 189$ km/h.

The transmitted energy per bit to noise power ratio E_b/N_0 is calculated as

$$\frac{E_b}{N_0} = \frac{E_s}{N_0} - 10\log_{10}RQ \quad (4.2)$$

where R denotes the coding rate, Q is the modulation order and E_s represents average energy per transmitted symbol. Received energy per bit to noise power ratio can be obtained by multiplying N with E_b/N_0 value that we use in simulation results.

An universal upper bound for the power of ICI caused by Doppler spread with unit power signal is calculated as [8]

$$P_{\text{ICI}} \leq \frac{1}{12}(2\pi f_{D,\max}T_s)^2 \quad (4.3)$$

which makes the ratio of the transmitted energy per bit from one user to the energy of ICI received from M users in the worst scenario equal to

$$\frac{E_b}{E_{\text{ICI}}} = 34.8 - 10\log_{10}MRQ \text{ (dB)} \quad (4.4)$$

for $f_{D,\max}T_s = 0.01$. Even for $M=8$ users, $R=1/4$ and $Q=6$ (64QAM), E_b/E_{ICI} is equal to 24 dB which is much bigger than E_b/N_0 values used in simulation results so that ICI does not affect the system performance in our case.

In GSIR with perfect channel state information case, abbreviated as (PCSI), μ_h is set to known value and σ_h is set to zero. Except for the channel estimation, same process with GSIR are applied. In PCSI, receiver does not perform channel estimation, only performs symbol estimation and data detection.

The multiuser MIMO-OFDM system with M users and N receive antennas is denoted by $M \times N$ MIMO-OFDM. The number of subcarriers and symbols in the MIMO-OFDM frame used in simulations are taken to be $L = K = 32$. Ten iterations are performed in both GSIR and PCSI.

4.1 BER Performance of GSIR versus Non-iterative ML and MRC

The BER performance of the proposed algorithm is compared to non-iterative Maximum Likelihood (ML) and Maximum-Ratio Combining (MRC) algorithms in which

repetition code (RC) with rate $1/4$ is used as channel code for all algorithms. The BER curves are shown in Fig. 4.1. For BPSK transmission, MRC with channel knowledge achieves the best performance while 1×8 PCSI and 8×8 PCSI performs as well as MRC. Despite ML is more complex than PCSI, PCSI outperforms ML with channel knowledge by about 1 dB. Although GSIR performs additionally channel estimation, the performance degradation of GSIR w.r.t. ML is roughly 1 dB for a training spacing of $D_t = D_f = 4$,

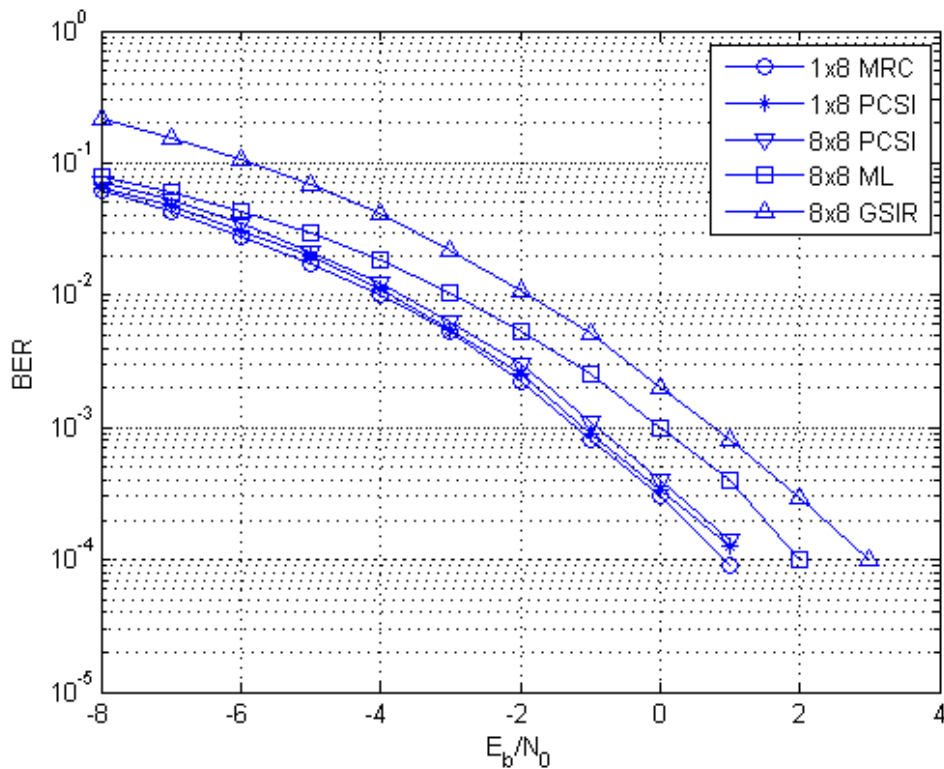


Figure 4.1: BER performance of GSIR versus other algorithms

4.2 BER Performance versus Number of Iterations

The BER performance of GSIR with BPSK versus number of iterations can be seen in Fig. 4.2. A repetition code with rate $1/4$ is utilized as a channel code. For a training spacing of $D_t = D_f = 4$ and $E_b/N_0 = 0$, it can be seen that BER performance of the 8×8 GSIR is improved in each iteration. After 5 iterations, BER values are roughly the same.

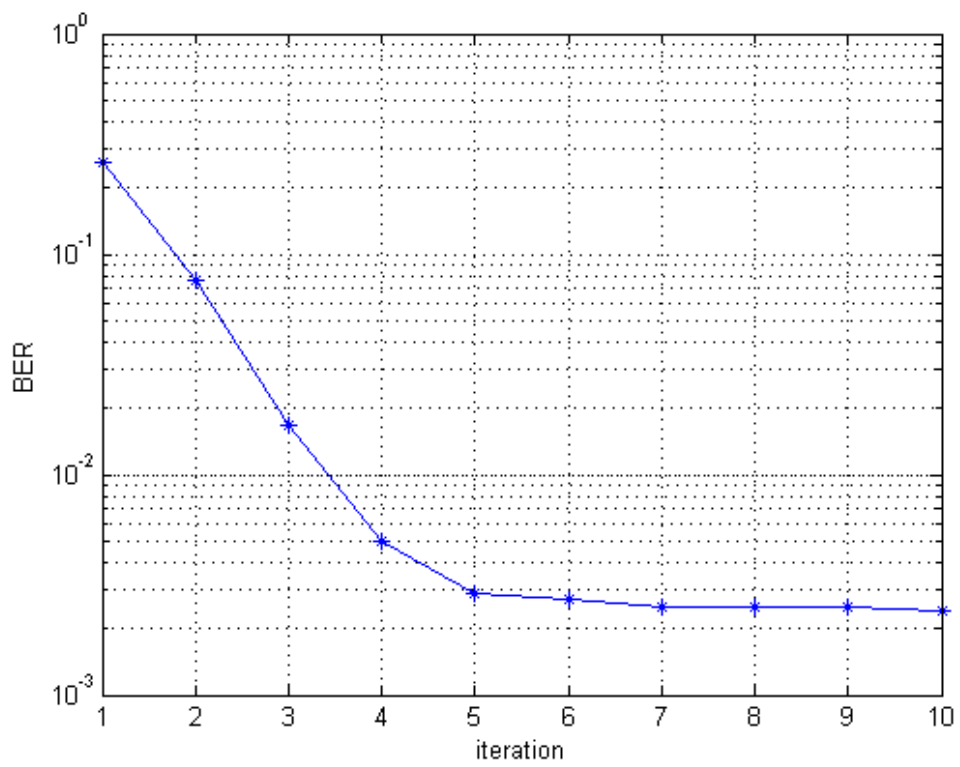


Figure 4.2: BER performance of 8×8 GSIR versus number of iterations

4.3 Channel Estimation versus Number of Iterations

The channel estimation performance of 8×8 GSIR with BPSK versus number of iterations can be seen in Fig. 4.3. A repetition code with rate $1/4$ is utilized as a channel code. Mean square error(MSE) of channel coefficients are used to compare performance where MSE is calculated through

$$|e_h|^2 = |h - \mu_h|^2 \quad (4.5)$$

For a training spacing of $D_t = D_f = 4$ and $E_b/N_0 = 0$, it can be seen that channel estimation of the 8×8 GSIR becomes more accurate in each iteration. It is observed that, as in BER values, MSE values are roughly the same after 5 iterations.

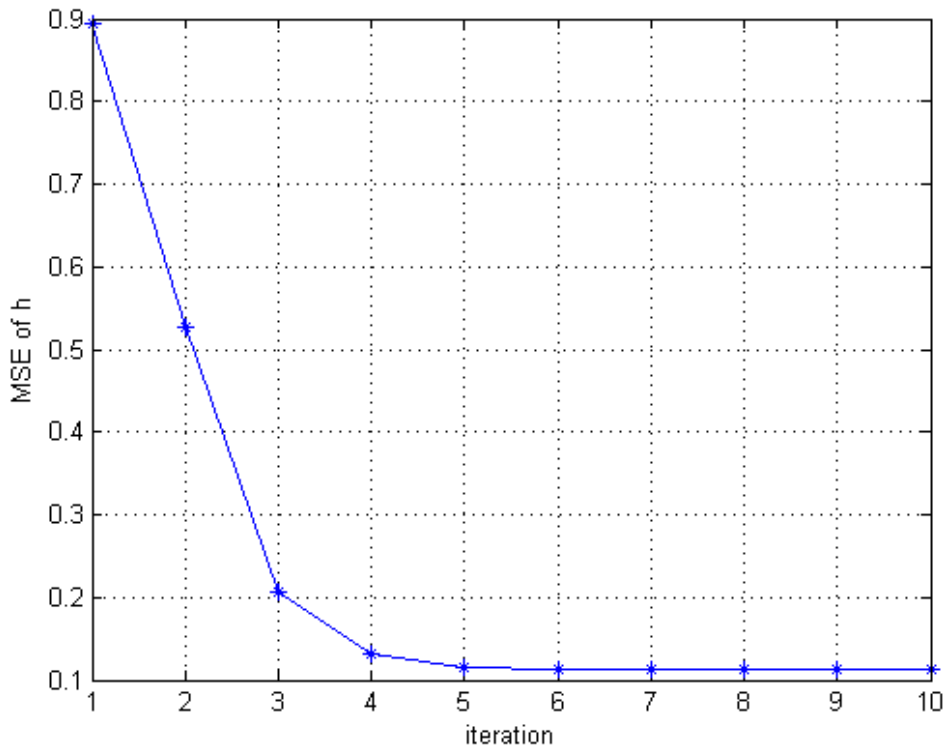


Figure 4.3: Channel estimation versus number of iterations

4.4 BER Performance of GSIR with Different Training Spacing

The BER performance of 8×8 GSIR with different training spacing can be seen in Fig. 4.4. A repetition code with rate $1/4$ is used and BPSK transmission is applied. It can be seen that increasing training symbol spacing affects the channel estimation negatively and decreases the performance of the GSIR. For $D_t = D_f = 16$, training symbols are inadequate for channel estimation and increasing the E_b/N_0 does not improve the BER performance.

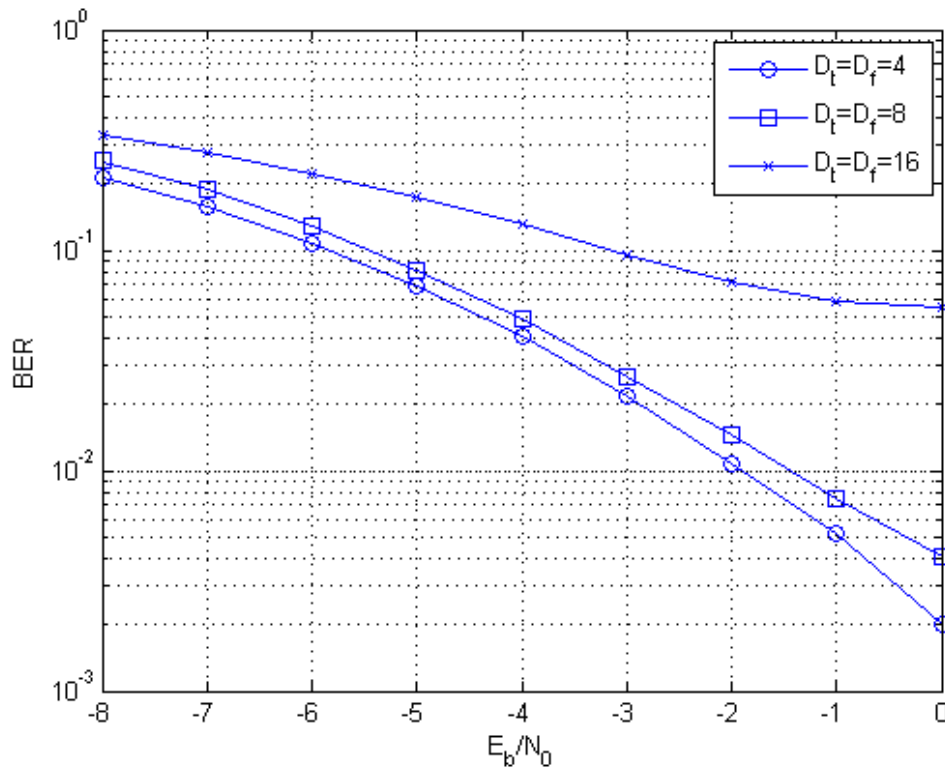


Figure 4.4: BER performance of GSIR with different training spacing

4.5 BER Performance of GSIR for Different Channel Models

The BER performance of 8×8 GSIR for different channel models can be seen in Fig. 4.5. A repetition code with rate $1/4$ is used and BPSK transmission is applied. Training symbol spacings are taken to be $D_t = D_f = 4$. The Winner channel model in [7] is utilized where exponential power delay profile in time domain and Jakes power

spectral density in frequency domain are used. Although the channel estimation performance in the Winner model is 1 dB worse than the uniform model due to the lower correlation between coefficients, it is proved that GSIR is applicable to different channel models and differently distributed parameters both in time and frequency domain.

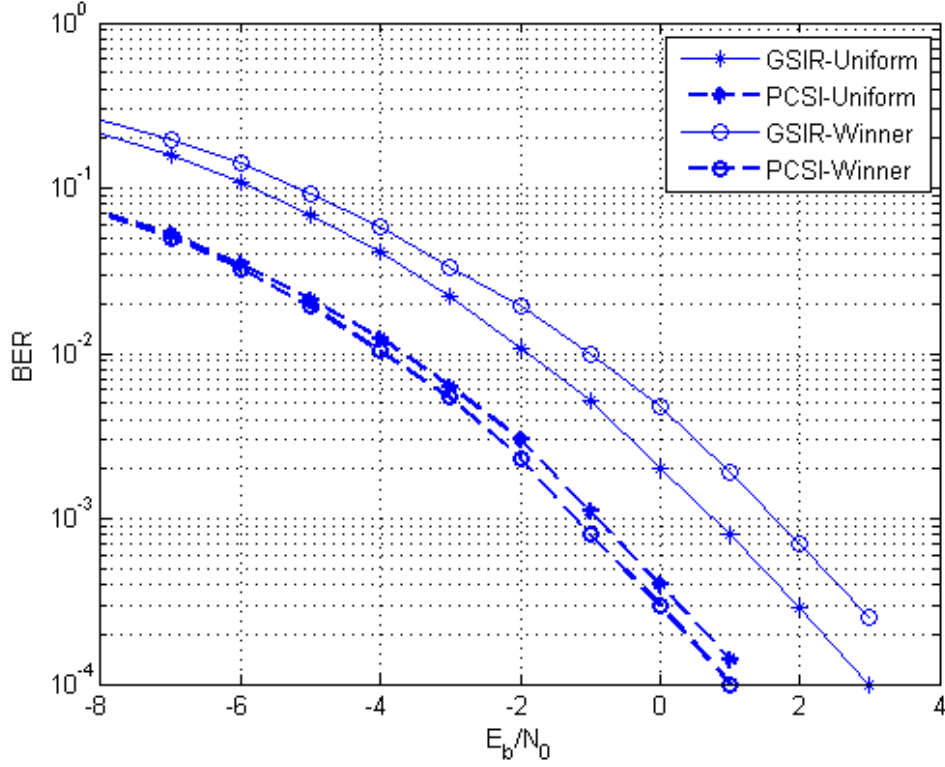


Figure 4.5: BER performance of GSIR for different channel modes

4.6 BER Performance of GSIR with Different Number of Users and Receive Antennas

The BER performance of GSIR with different number of users and receive antennas can be seen in Fig. 4.6. A repetition code with rate 1/4 is utilized and BPSK transmission is applied. Training symbol spacings are taken to be $D_t = D_f = 4$. Since received power increases with the number of receive antennas at the same time, BER performance improved even with high interference. On the other hand, it is observed that channel estimation performance degrades due to the increasing number of users. Although the performance degradation of 32×32 GSIR w.r.t. 32×32 PCSI is roughly

4 dB, which is worse than 8×8 and 16×16 cases, the results suggest that GSIR for large-scale system is applicable.

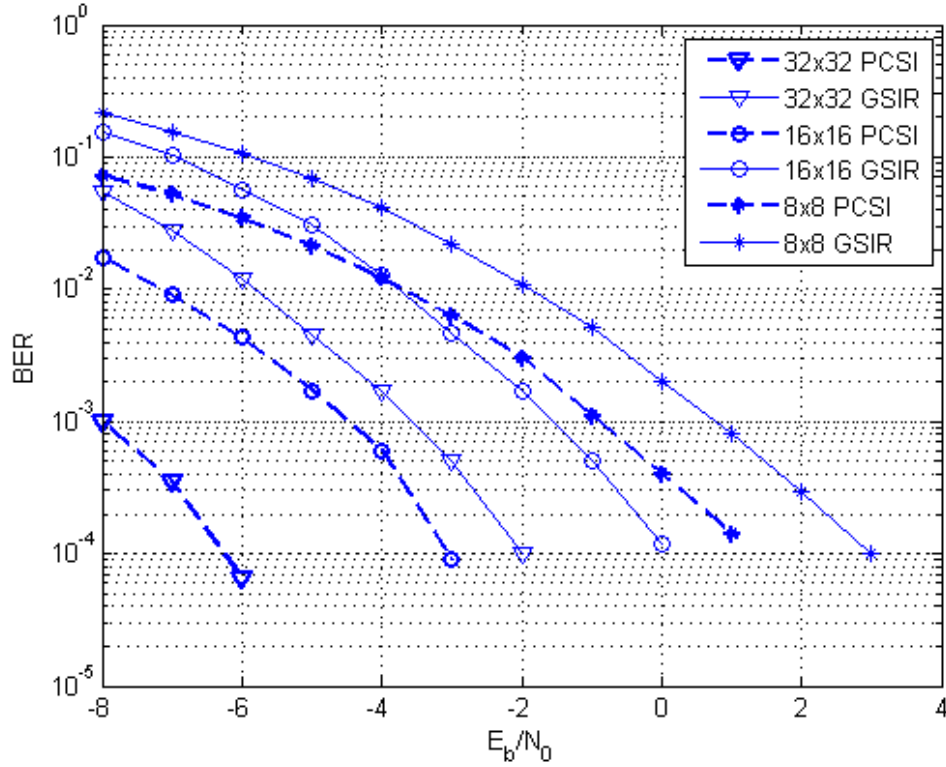


Figure 4.6: BER performance of GSIR with different number of users and receive antennas

4.7 BER performance of GSIR with Different Code Rates

The BER performance of 8×8 GSIR with different code rates can be seen in Fig. 4.7. BPSK transmission is applied and training symbol spacings are taken to be $D_t = D_f = 4$. Decreasing rate of the repetition code does not affect the performance but it is observed that at least 3 repetitions are needed to perform GSIR properly. GSIR with rate $1/2$ and 1 does not work well.

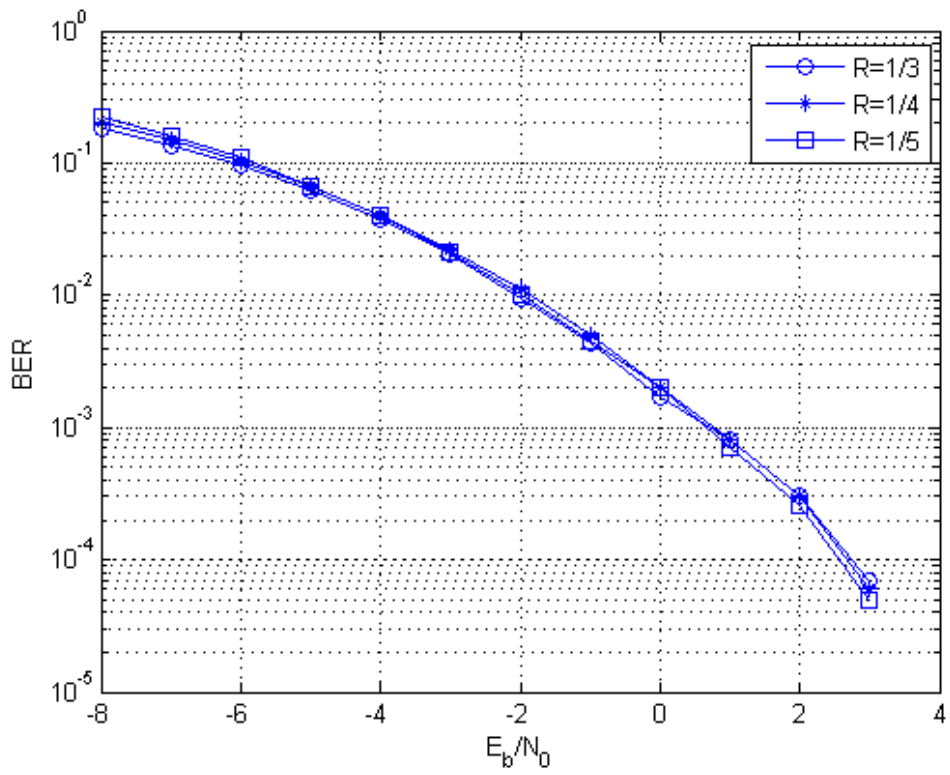


Figure 4.7: BER performance of GSIR with different code rates

4.8 BER performance of GSIR with Different Constellations

The BER performance of 8×8 GSIR with different constellations can be seen in Fig. 4.8. A repetition code with rate $1/4$ is utilized and training symbol spacings are taken to be $D_t = D_f = 4$. PCSI with BPSK and QPSK have the same performance as expected but QPSK outperforms BPSK in GSIR due to the high SNR which yields a better channel estimation. Although increasing modulation order more than QPSK improves channel estimation at a given E_b/N_0 , it is observed that BER performance is not improved. The performance degradation of GSIR w.r.t. PCSI is roughly 3 dB in 16QAM and 6 dB in 64QAM.

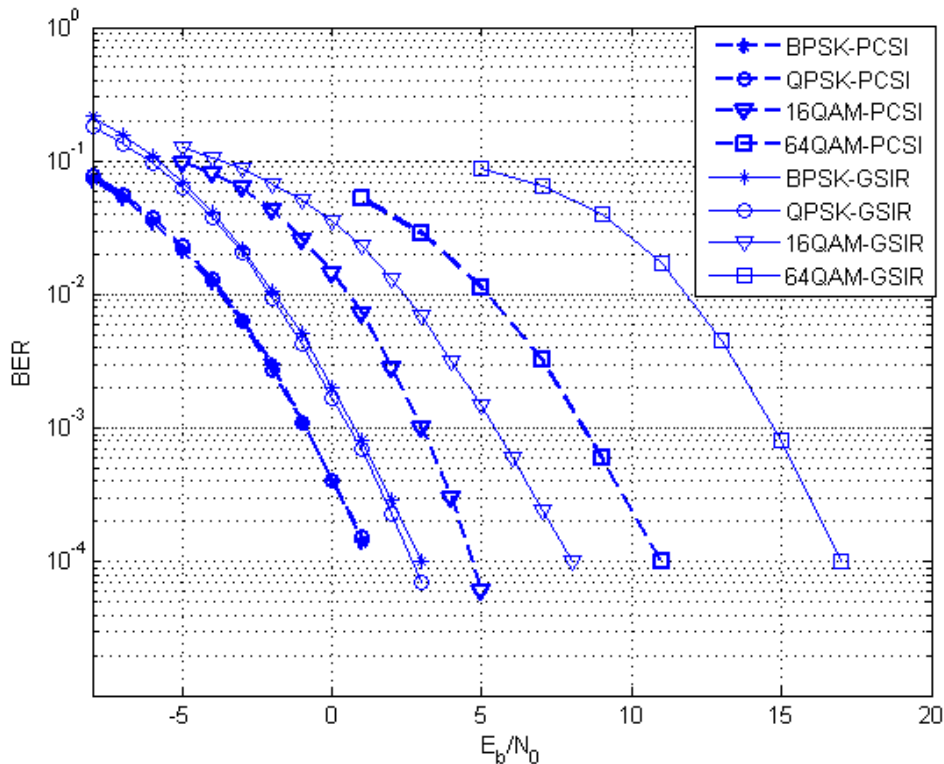


Figure 4.8: BER performance of GSIR with different constellations

4.9 BER performance of GSIR with Different Number of Users

The BER performance of GSIR with different number of users can be seen in Fig. 4.9. A repetition code with rate $1/4$ is utilized and training symbol spacings are taken

to be $D_t = D_f = 4$. The energy of effective noise is increased with the number of users and it causes performance degradation as expected. It is seen that performance of GSIR is affected more by high order modulations. Adding 2 users to the system decreases the performance by 1 dB in 16QAM hence it is 2 dB in 64QAM.

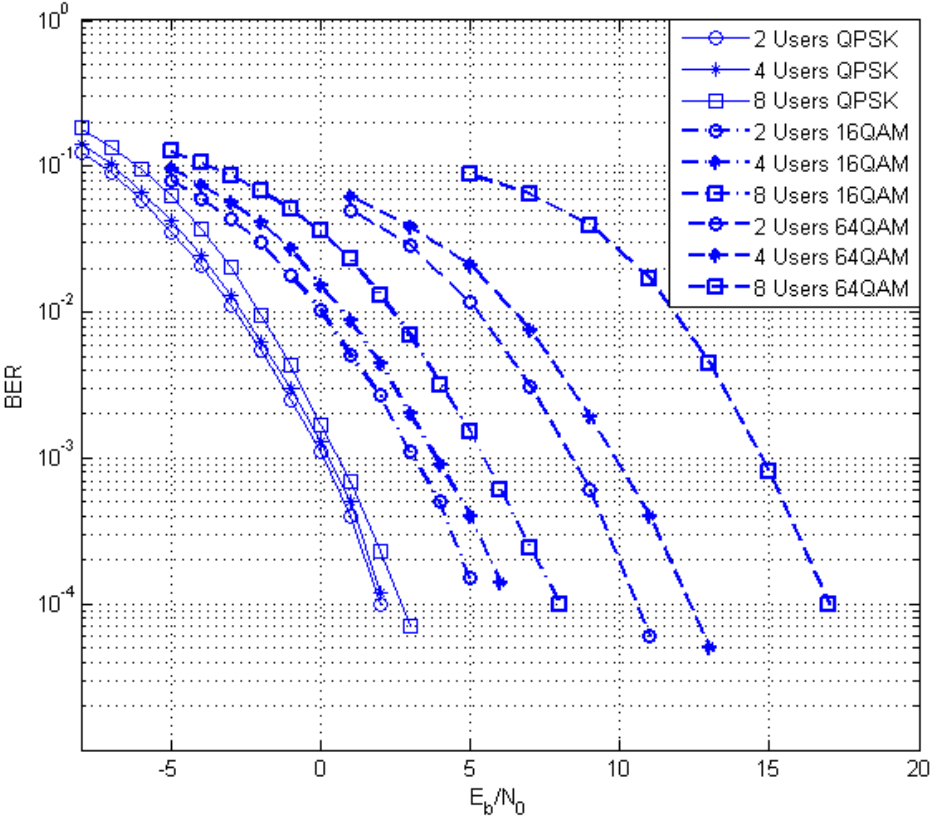


Figure 4.9: BER performance of GSIR with different number of users

4.10 BER Performance of GSIR in Combination with LDPC

The BER performance of 8×8 GSIR in combination with LDPC can be seen in Fig. 4.10. A repetition code with rate $1/3$ and an LDPC code with rate $3/4$ is used in cascade with an overall code rate of $1/4$. Training symbol spacings are taken to be $D_t = D_f = 4$ and BPSK transmission is applied. While GSIR have a better performance at low E_b/N_0 , GSIR with LDPC outperforms GSIR by about 1.5 dB at $BER=10^{-4}$. Also it is observed that performance degradation of GSIR with LDPC w.r.t. PCSI with LDPC is 2.5 dB which means that channel estimation performance

of GSIR with LDPC is 0.5 dB worse than GSIR, which is due to the lower operation SNR.

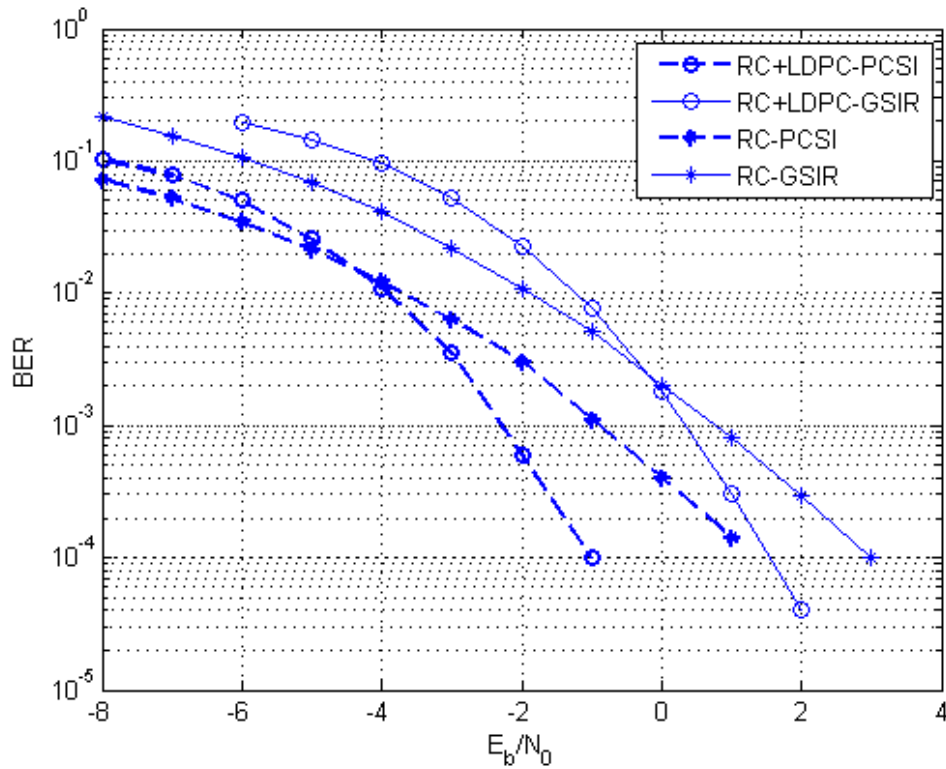


Figure 4.10: BER performance of GSIR in combination with LDPC

4.11 BER Performance of GSIR in Combination with LDPC for Different Number of Users

The BER performance of GSIR with LDPC for different number of users can be seen in Fig. 4.11. As a channel code RC with rate $1/3$ and LDPC with rate $3/4$ is used in cascade with a total code rate of $1/4$. Training symbol spacings are taken to be $D_t = D_f = 4$ and BPSK transmission is applied. The BER performance of GSIR with LDPC degrades with the increasing number of users as expected but still acceptable performance is observed.

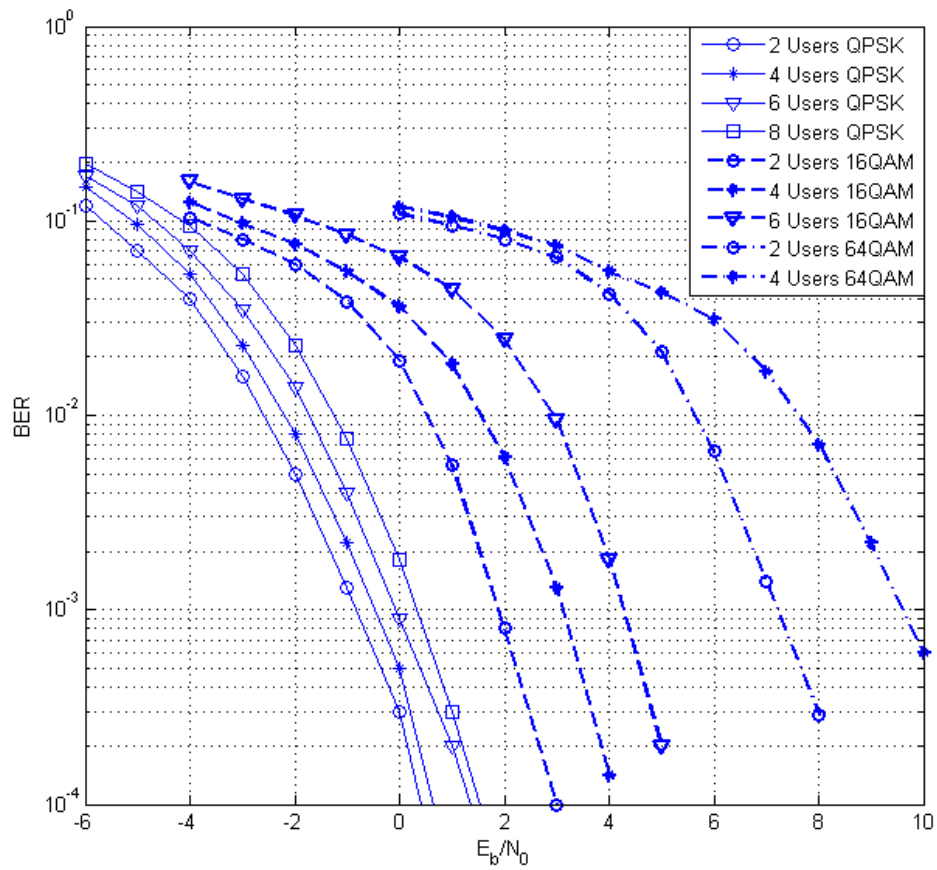


Figure 4.11: BER performance of GSIR in combination with LDPC for different number of users

CHAPTER 5

CONCLUSION AND FUTURE WORKS

In this study, a graph-based iterative receiver is proposed for multiuser MIMO-OFDM system over time-varying frequency selective channels. Joint channel estimation and data detection are applied which provide flexibility to a communication system. Messages, comprising mean values and variances of estimations, are successfully generated and distributed to the whole factor graph by transfer nodes. Messages, which transmit channel and symbol information, are efficiently refined in each iteration starting with training symbols known at the receiver.

Instead of bits, symbols are repeated in a MIMO-OFDM frame and symbol probabilities are utilized in message exchange so that a low-complexity receiver is obtained especially in high order modulations. Message passing schedule in [7] is rearranged and effects of short-cycles are mitigated which provides a better performance.

In addition, a new training structure is proposed which enables channel estimation for large-scale MIMO. Training symbol rate remains the same with increasing number of users which makes the receiver capable of decoding the data of numerous users at once (e.g., 32×32).

Even though, GSIR can operate only in low code rates (max. $1/3$) which decreases the spectral efficiency, throughput can be improved by adding numerous users and using high order modulation with low-complexity provided by the proposed algorithm. Repetition code is a basic error-correcting code, however the performance of GSIR can be improved by using an effective FEC code such as LDPC.

Simulation results show that, PCSI has a similar performance with MRC and outper-

forms non-iterative ML with channel knowledge. The performance of GSIR is increased with the number of receive antennas. Adding more users affects the channel estimation negatively and degrades the BER performance. High order modulations are applicable for GSIR but the performance difference between GSIR and PCSI increases with modulation order. The total performance is improved by using GSIR in combination with LDPC.

As a future study, initial channel estimates can be improved by interpolation and filtering over channel taps in time domain. This approach may help reduce the required iteration number to reach a desired BER and the overall performance of GSIR could come closer to the perfect channel state information case. The BER performance of GSIR with different $f_{D,max}T_s$ values can be analyzed. In addition the correlation between channel coefficients in spatial domain can be taken into account, so that channel estimation performance could be enhanced. The sensitivity of GSIR to imperfection on correlation knowledge may be inspected.

REFERENCES

- [1] H. Bolcskei. MIMO-OFDM wireless systems: Basics, perspectives and challenges. *IEEE Wireless Communications*, pages 31–37, August 2006.
- [2] J. Cavers. An analysis of pilot symbol assisted modulation for rayleigh fading channels. *IEEE Trans. Veh. Technol.*, 40(4):686–693, Nov. 1991.
- [3] A. Goldsmith. *Wireless Communications*. Stanford University Press, 2005.
- [4] P. Hoeher. A statistical discrete-time model for the WSSUS multipath channel. *IEEE Trans. Veh. Technol.*, 41(4):461–468, Nov. 1992.
- [5] J. Hoydis. Massive MIMO in the UL/DL of cellular networks: How many antennas do we need? *IEEE J. Sel. Areas Commun.*, 31(2):160–171, Feb. 2013.
- [6] M. N. Kaynak, T. M. Duman, and E. M. Kurtas. Belief propagation over SISO/MIMO frequency selective fading channels. *IEEE Trans. Wireless Commun.*, 6(6):2001–2005, Jun. 2007.
- [7] C. Knievel. Multi-dimensional graph-based soft iterative receiver for MIMO-OFDM. *IEEE Transactions on Communications*, 60(6):1599–1609, June 2012.
- [8] Y. Li. Bounds on interchannel interference of OFDM in time-varying impairments. *IEEE Trans. on Communications*, 49(3):401–404, March 2001.
- [9] H.-A. Loeliger. Factor graphs and the sum-product algorithm. *IEEE Tans. Inf. Theory*, 47(2):843–849, Feb. 2001.
- [10] H.-A. Loeliger. The factor graph approach to model-based signal processing. *Processing of the IEEE*, 95(6):1295–1322, June 2007.
- [11] T. Marzetta. Noncooperative cellular wireless with unlimited number of base station antennas. *IEEE Trans. Wireless Commun.*, 9(11):3590–3600, Nov. 2010.
- [12] H. Niu. A factor graph approach to iterative channel estimation and LDPC decoding over fading channels. *IEEE Trans. on Wireless Communications*, 4(4):1345–1350, July 2005.
- [13] C. Novak, G. Matz, and F. Hlawatsch. Factor graph based design of an OFDM-IDMA receiver performing joint data detection, channel estimation, and channel length selection. *IEEE Int. Conf. Acoustics, Speech, Signal Processing*, pages 2561–2564, 2009.

- [14] P. Som and T. Datta. Low-complexity detection in large dimension MIMO-ISI channels using graphical models. *IEEE J. Sel. Top. Signal Process*, 5(8):1497–1511, Dec. 2011.
- [15] N. Srinidhi. Layered tabu search algorithm for large-MIMO detection and a lower bound on ML performance. *IEEE Trans. Wireless Commun.*, 59(11):2955–2963, Nov. 2011.
- [16] G. Stüber. Broadband MIMO-OFDM wireless communications. *Proc. IEEE*, 92(2):271–294, Feb. 2004.
- [17] E. Telatar. Capacity of multi-antenna gaussian channels. *Eur. Trans. Telecomm.*, 10(6):585–595, 1999.
- [18] D. Tse. *Fundamentals of Wireless Communication*. Cambridge University Press, 2005.
- [19] A. P. Wornen and W. E. Stark. Unified design of iterative receivers using factor graphs. *IEEE Trans. Inf. Theory*, 47(2):843–849, Feb. 2001.
- [20] S. Wu. Low-complexity iterative detection for large scale multiuser MIMO-OFDM systems using approximate message passing. *IEEE Journal of Selected Topics in Signal Processing*, 8(5):902 – 915, October 2014.
- [21] Y. Xie. Two em-type channel estimation algorithms for OFDM with transmitter diversity. *IEEE Trans. Commun.*, 51(1):106–115, Jan. 2003.
- [22] J. Ylionias. Iterative joint detection, decoding and channel estimation in turbo-coded MIMO-OFDM. *IEEE Trans. Veh. Technol.*, 58(4):1784–1796, May 2009.
- [23] Y. Zhu, D. Guo, and M. L. Honig. A message-passing approach for joint channel estimation, interference mitigation and decoding. *IEEE Trans. Wireless Commun.*, 8(12):6008–6018, Dec. 2009.